A Topographic Analysis of Human Scalp Alpha EEG by the Complex-valued ICA

Master Thesis

A Topographic Analysis of Human Scalp Alpha EEG by the Complex-valued ICA

複素独立成分分析による ヒト脳波アルファ波のトポグラフ解析

Zhan Zhang
Laboratory of Biomodeling,
Department of Applied Information Sciences,
Graduate School of Information Sciences (*GSIS*),
Tohoku University
2010. 2

Supervisor: Professor Mitsuyuki Nakao

Contents

Chapter 1 Introduction

1.1 Purpose of this research

In factors that lead to traffic accidents, driver's sleepiness is one of the most important factors [1]. In Japan, it is reported that 3.77% of taxi drivers have experienced accident related to sleepiness [2]. Sleepiness caused by a plurality of factors such as long distance drive on highways, a feeling of boredom and monotony that lead to impatience and fatigue, or after-meal drowsiness. The sleepiness may cause impairment of alertness of the driver, reacting slowly to driving situations, attention deficit so that it is very dangerous to drive under such condition and may result in serious injury or fatal accident. Thus there is a need to have a safe, high-reliable, real time monitoring system to detect driver's drowsiness and make warning the driver to avoid accidents. Since electroencephalographic (EEG) signal directly reflects human brain activity, many researchers have attempted to find the sign of sleepiness from EEG signals. So far, it has been reported that the alpha band (8-13 Hz) EEG activity increased during night driving relative to the daytime levels for the sleepy group [3]. In some driving simulation studies, it was found that the occurrence of brief paroxysmal bursts of EEG alpha activity and an increased synchrony among EEG channels before the driving errors [4]. Thus it is suggested that alpha EEG signal would be useful for prediction of sleepiness level.

The alpha band rhythmic EEG activity (alpha rhythm) has been classified into at least three categories: occipital alpha rhythm [5], Rolandic μ rhythm [6], and so-called third rhythm [7]. Due to the different location of these alpha rhythm generators, the spatial distribution of alpha source would provide information about the state of subject. However, since the alpha activities are observed in a mixed signal, decomposition of the signal is required.

Recently, independent component analysis has been applied to solve the EEG decomposition. It must be noted that the major ICA-based method for EEG decomposition pre-requires that the signal mixing process is instantaneous and linear. If the observed signal contained delayed source signal, it is impossible to decompose the

source signal accurately. In fact, alpha EEG activity recorded at different scalp areas show phase difference; therefore, that the instantaneous mixing assumption would be violated.

In this study, we propose a method to decompose the time-delayed mixture of alpha EEG source signals with phase delay by using the time-frequency analysis and complex-valued ICA. The method is applied to the human scalp EEG data to decompose the alpha EEG activities occur associated with the subjective sleepiness during a driving simulation task.

1.2 Structure of this document

This document consists of five chapters.

In chapter 1, social problem of sleepiness during the driving is discussed and the general purpose of this research is stated.

In chapter 2, the background of this research is presented. At the first section, research results based on accident related to sleepiness in some countries are presented. The next section describes the methods for recording and classification of EEG signals. The last section provides a short review of the past research about relationship between sleepiness and EEG signals, especially the alpha rhythm. The problem of the past research is also pointed out in this section.

In chapter 3, materials and methods are described. First, driving simulation system and characteristic of recorded signals are explained. Rest of this chapter is about the analysis methods used in this study.

In chapter 4, the results of artifacts removal and comparison between real-valued and complex-valued ICA are presented. We compared results by both real-valued and complex-valued ICA in power and phase difference on the scalp and found the useful method to analyze alpha rhythm. The relationship between sleepiness and alpha rhythm was described.

In chapter 5, conclusion of this research is presented.

Chapter 2 Background

2.1 Sleepiness during driving

The sleepiness occurs during the driving may lead to errors and increase the risk of accidents. Nilsson *et al*. believe that sleepiness is a major contributing factor to errors made by drivers [8]. The effect of sleepiness, caused by long hours of continuous driving, a monotonous driving environment and driving during the night or early morning hours, leads to driver performance degradation [9]. Sleepiness reduces reaction time (a critical element of safe driving). It also reduces vigilance, alertness and concentration. The speed at which information is processed is also reduced by sleepiness. The quality of decision-making may also be affected.

Research in many countries indicates that driver fatigue is a serious problem [10, 32]. A recent study by the Sleep Research Centre of UK indicates that driver sleepiness causes up to 20% of accidents on monotonous roads. In the USA, several studies in recent years have produced various estimates of the level of sleep related road accident. The National Highway Traffic Safety Administration estimates that there are 56,000 sleep related road crashes annually, resulting in 40,000 injuries and 1,550 fatalities. VicRoads, an Australian road safety organization, estimates that 25%-35% (and possibly up to 50) of road crashes are sleep related in Australia. In Germany, a study of motorway accidents in Bavaria estimated that 35% of fatal motorway crashes were due to reduce vigilance (driver inattention and sleepiness). 20% of night-time accidents involved driver sleepiness was reported in Norway.

In professional drivers such as truck drivers, sleepiness may be quite severe. Driver sleepiness is a particular problem for truck drivers. A 1998 American study found that about 20% of all fatal crashes and fatalities and 10% of all injuries involving a long-haul truck occurred between mid-night and 6 am, the peak period for driver sleepiness [11]. These crashes tended to be more severe than crashes during other parts of the day. In another study, 593 truck drivers were interviewed at New York's highway. Nearly two-third reported episodes of drowsy driving within the previous month, and almost 5% said that they drove when sleepy on most days [12].

Driver sleepiness is considered a significant risk factor for car crash injuries, thus the development of method to detect the sign of sleepiness and alerting the driver in real-time about the onset of sleepiness is necessary for reducing the number of people killed and seriously injured in road accidents.

2.2 EEG signals

Electroencephalography (EEG) is the recording of electrical activity along the scalp produced by the firing of neurons within the brain. The electrical activity of the brain can be described in spatial scales from the currents within a single dendritic spine to the relatively gross potentials that the EEG records form the scalp [13]. The human EEG was first discovered by Germany physiologist and psychiatrist Hans Berger. He named the first rhythmic EEG activity he saw the alpha wave [5]. Alpha is in the 8-13Hz range seen in the posterior regions of the head on both sides, being higher in amplitude on the dominant side (Figure 2.1). It is typical of the resting condition and disappears when the subject perceives a sensory signal or when he/she makes mental efforts.

The usual classification of the main EEG signals based on their frequency ranges is delta rhythm (0.5-4 Hz), theta rhythm (4-7 Hz), alpha rhythm (8-13 Hz), beta rhythm (13-30 Hz), gamma rhythm (30Hz-) (Figure 2.2) [13].

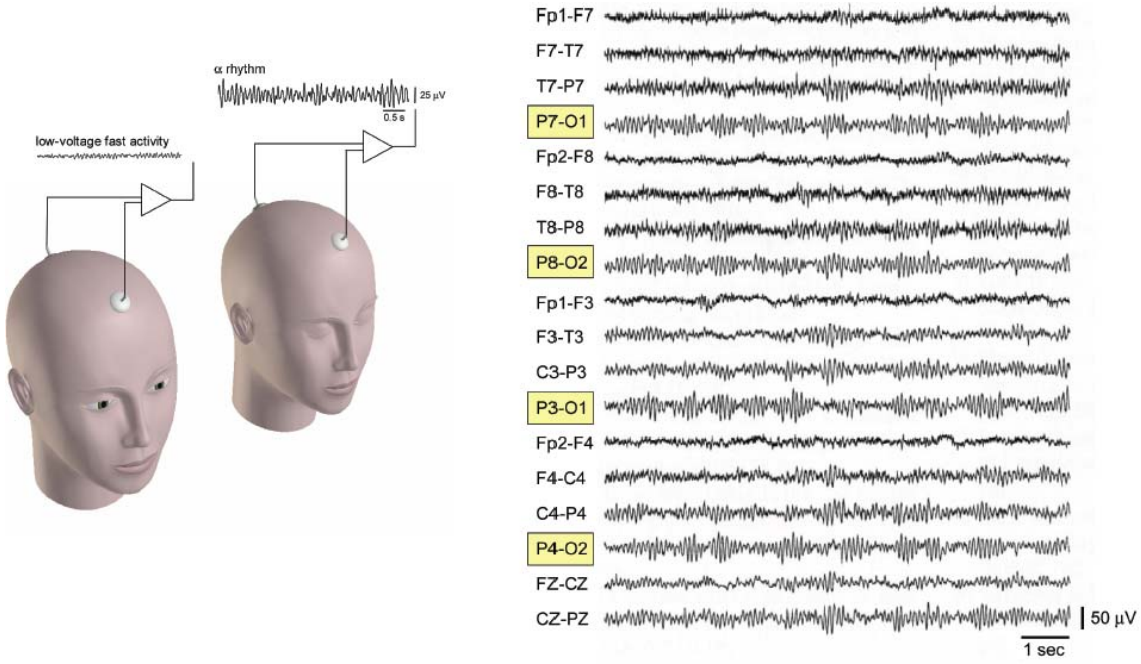

Figure 2.1 When the subject closed eyes, the contemporary multichannel EEG recording showing the highest amplitude of alpha activity in traces derived from occipital electrodes. (i.e., O1 and O2) [14]

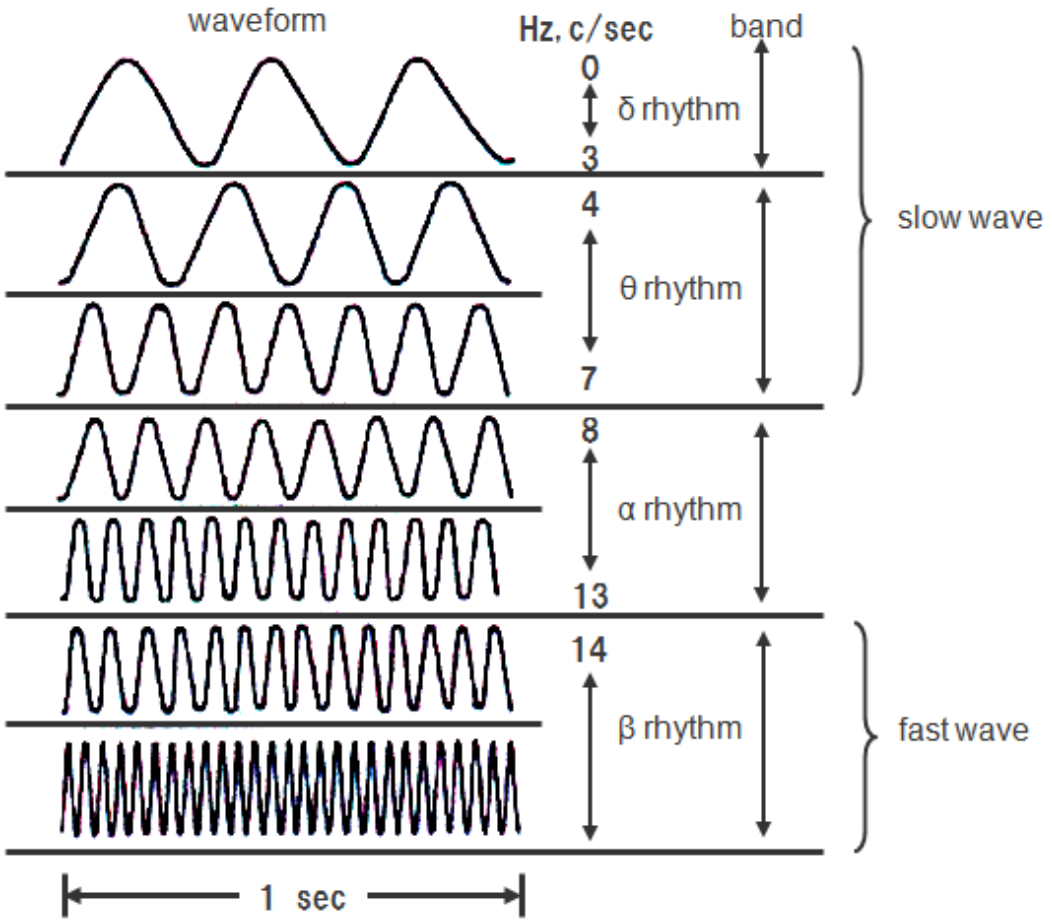

Figure 2.2 EEG rhythm patterns [26]

2.3 Sleepiness and EEG

2.3.1 Relationship between sleepiness and EEG

Since EEG signals reflect directly human brain activity, EEG signals were considered as the most predictive and reliable measurements. A number of studies have been performed in drivers concerning the EEG alteration due to sleepiness.

In 1987, Torsvall and Akerstedt recorded ambulatory EEG and EOG from train drivers during a night and day trip and they observed that alpha power increased during night driving relative to the daytime levels for the sleepy group [15]. Other changes such as distribution, amplitude and frequency of alpha rhythm have also been emphasized by Santamaria and Chiappa at the same year [16]. In their research, they observed an increase in the amplitude of central frontal alpha rhythm lasting 1-10-sec, while decrease in the amplitude of the occipital alpha rhythm at the onset of sleepiness. They also found another change during the sleepiness that the appearance or persistence

of mid- or posterior-temporal alpha, lasting several second after occipital alpha had already disappeared. The change in alpha rhythm distribution was also found by Lal and Craig Later [17]. Markand observed in 1990 that with the onset of drowsiness, the alpha rhythm may attenuate or diminish for a few seconds, reappear again, and go through this alteration for a few minutes until the trains of alpha rhythm finally disappear at the onset of sleep [18]. In recent research of Christos et al., they observed the increase of power and 1-2 sec paroxysmal bursts of alpha rhythm in the central and parietal brain regions before the driving event that appears more dominant almost half second before the driving error onset (Figure 2.3) [4].

Lots of researches indicate that changes of alpha rhythm power and distribution, so we focus on the possibility that alpha rhythm predict the onset of sleepiness in this study. Actually, the different distribution of alpha rhythm on the scalp does not generated by the same source. Different spatial localization indicates different category of alpha rhythm. Currently, alpha rhythm in humans can be placed into 3 main categories [33]. Many subjects exhibit a prominent occipital alpha rhythm [5], which is attenuated by eye opening. This rhythm dominates the EEG during relaxed wakefulness and makes the largest contribution to alpha band power during this behavioral state. A distinct alpha rhythm of human subjects is also obversed over central cortical areas. This rhythm, termed the Rolandic mu rhythm [6], could be blocked by appropriate motor movements or somatosensory stimuli. In addition, a third rhythm is present over the mid-temporal region [7], which is differentially sensitive to auditory stimuli, mental arithmetic, and other types of cognitive effort between different subjects.

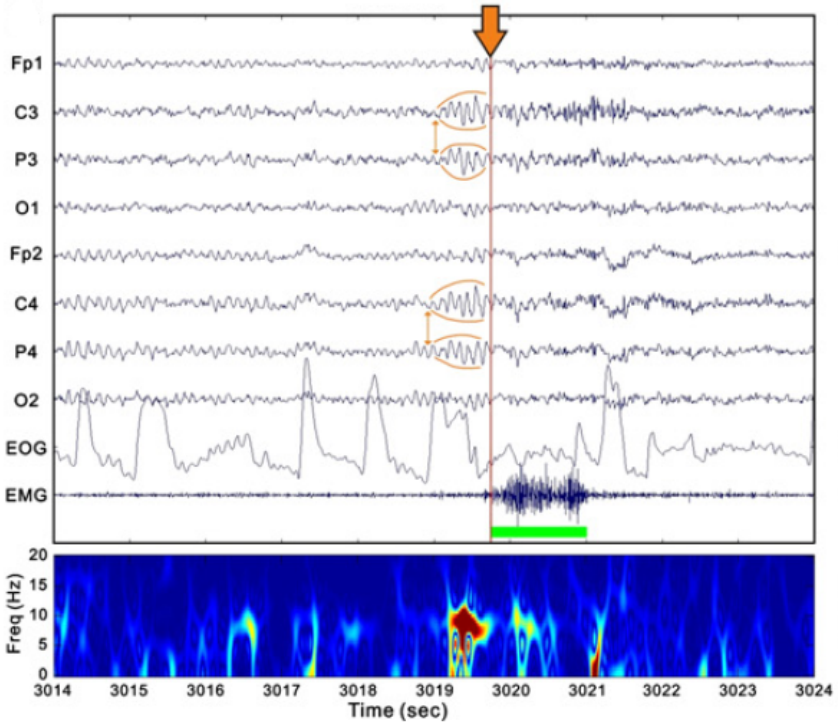

Figure 2.3 The traces of eight-channel EEG, EOG and EMG before and after a sever driving error. At the bottom of time traces panel, the time-frequency map representation of channel C3 is shown. The orange line is the onset of driving error [4].

2.3.2 Source separation of EEG signals

Independent component analysis (ICA) is useful in analyzing brain signals and in particular EEG data. ICA is a computational method for separating a multivariate signal into additive subcomponents supposing the mutual statistical independence of the non-Guassian source signals. Its main applications are blind source separation (BSS).

Assume that independent n-source signals

$$\boldsymbol{s}(t) = [s_1(t), \ldots, s_n(t)]^T \tag{2.1}$$

are recorded with an m-channel electrode

$$\boldsymbol{x}(t) = [x_1(t), \ldots, x_n(t)]^T \tag{2.2}$$

where T represents transpose and t indicates time. Elements of both vectors (x and s) are real numbers. If the transformation from s(t) to x(t) is instantaneous (i.e., no delay) and linear mixture, the following relationship holds:

$$\boldsymbol{x}(t) = \boldsymbol{A}\boldsymbol{s}(t)$$

$$\boldsymbol{A} = \begin{pmatrix} a_{11} & a_{12} & \cdots & a_{1n} \\ a_{21} & a_{22} & \cdots & a_{2n} \\ \vdots & \vdots & \ddots & \vdots \\ a_{m1} & a_{m2} & \cdots & a_{mn} \end{pmatrix} \tag{2.3}$$

$\boldsymbol{A}$ is an unknown m×n full column rank whose elements are constant real numbers, which is called mixing matrix. If m = n, the system is regarded to satisfy complete condition. The basic problem of ICA is then to estimate both the mixing matrix A and the realizations of the s(t) using only observations of the mixture x(t).

Estimating the independent components can be accomplished by finding the right linear combinations of the mixture variables, since we can invert the mixing as

$$\boldsymbol{y}(t) = \boldsymbol{W}\boldsymbol{x}(t) \tag{2.4}$$

where unmixed signals $\boldsymbol{y}(t) = [y_1(t) , \ldots , y_n(t)]^T$ are called independent components (ICs). If $\boldsymbol{W} = \boldsymbol{A}^{-1}$, the source signals are completely reconstructed (Figure 2.4). However, since ICA cannot resolve ambiguity of amplitude and permutation of source signals, this relation generally does not hold. Parameters of this time-domain analysis are all real-valued, so we call it real-valued ICA.

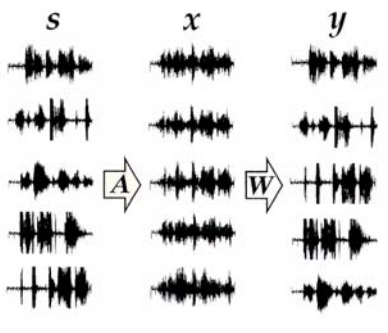

Figure 2.4 ICA model

2.3.3 Limitation of the past research

Real-valued ICA of EEG is carried out assuming a linear and instantaneous mixing process that can be expressed mathematically as multiplication by a single mixing matrix. This assumption does not take into account the possible phase shift dynamic between the sources and electrodes. But in fact, the same source signal has different phase delay in each observed signal due to the finite propagation speed in the medium. The phase patterns were divided into 2 forms, one is a gradual phase shift between frontal and occipital regions and the other is a stepwise phase shift in the central regions. In the research of J. Ito *et al*., they observed both the patterns over the entire scalp [20].

Figure 2.5 shows snapshots of these two patterns of phase difference. In their study, the phase difference is calculated as the relative phase at each site in relation to the phase at the PO3 site (between P3 and O1 in Figure 2.6). In our study, we got the alpha rhythm in real-valued after the EEG signals through alpha band-pass filter. After comparing the selected 3 channels from frontal to occipital (Fp2, C4, O2), we also observed the phenomenon of gradual phase shift among them in Figure 2.6.

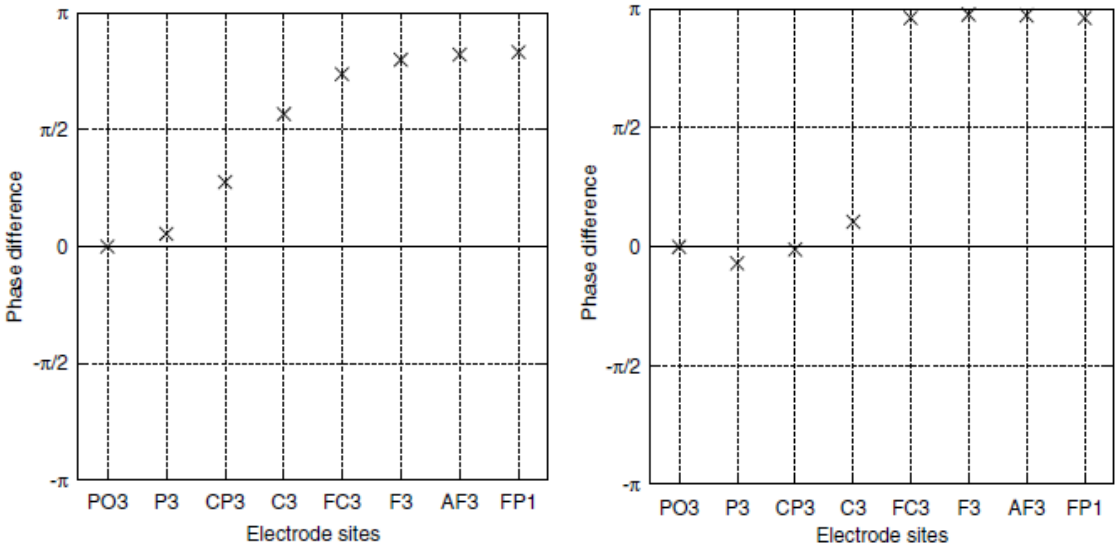

Figure 2.5 Snapshots of two typical phase patterns. The phase difference is shown as the relative phase at each site in relation to the phase at PO3 site. Left: phase pattern with a gradual shift. Right: phase pattern with a sudden shift [20].

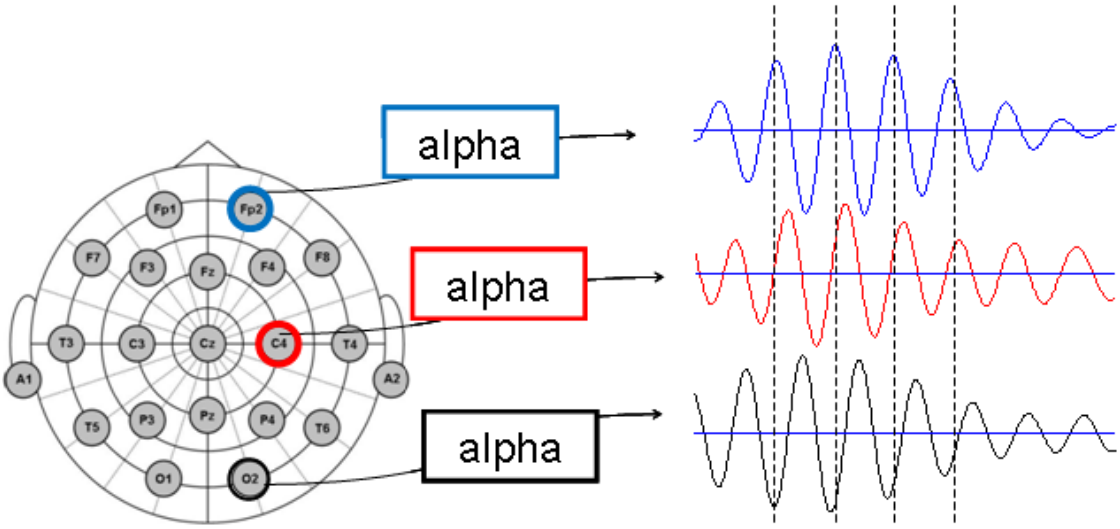

Figure 2.6 Alpha rhythm waveforms in the selected 3 channels (frontal, central and occipital) are shown. There is phase shift between either two of them [10].

These results strongly suggest that the assumption of real-valued ICA is not satisfied in the separation of EEG signals. Therefore we should assume a convolutive mixing model and separate EEG signals by using complex-valued ICA in time-frequency domain. We compare the separation results of alpha rhythm from real-valued ICA.

Chapter 3 Subjects and Methods

3.1 Driving simulation

The study was approved by the Committee on Ethics of Human Experiments at GSIS, Tohoku University. Thirteen healthy Japanese male subjects (31±8 years old) who gave written informed consent participated in this study.

3.1.1 The simulation equipment

The subjects were seated in a driving simulation system (Figure 3.1). The driving simulation system included driving simulator which was designed based on Toyota Crown, and screen with 3 m height and 3 m in front of the subject. During the simulation task, bio-signals including electroencephalography (EEG), driving performance and reaction time were recorded. In addition, facial expression of the subjects was recorded on digital video equipment during the driving simulation.

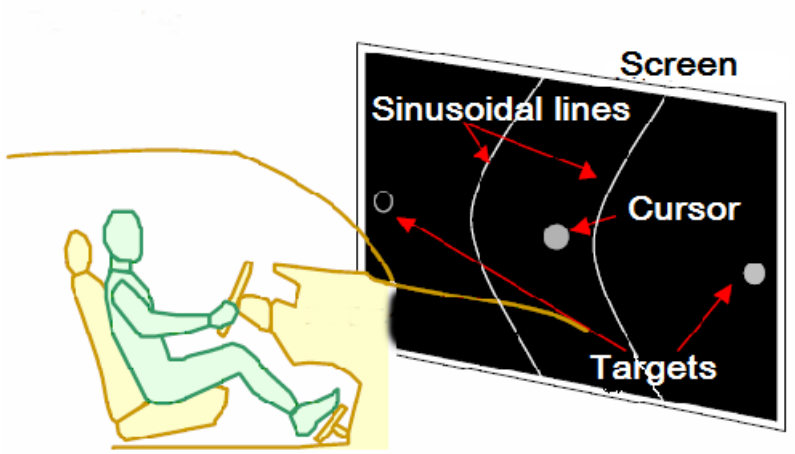

Figure 3.1 Schematics diagram of a driving simulator.

3.1.2 Tasks

On the screen in front of the subjects, a cursor (car) and two sinusoidal lines (road) were presented by a PC projector. The sinusoidal lines whose cycle time is 22.5-sec scrolled down at the speed of 13 cm/sec. The amplitude of sinusoidal line is 55 cm, and the interval between two lines is 36 cm. A steering wheel with a diameter of 40 cm was used by the subjects to control the cursor to the center of lines. During 128 cycles' driving simulation (2880-sec), the cursor track was recorded with sampling frequency at 16 Hz. Unlike the car keeps the direction of movement in reality, the cursor went straight when the subjects didn't move the wheel in this simulation.

During a simulation, either of the two rectangles (targets) on both sides of sinusoidal lines got on randomly 5 times in one cycle (22.5-sec) presented. The subjects were requested to press the button of the steering wheel as soon as possible in response to the twinkling of the target. We took the time period between target got on and button pushed as reaction time. If the reaction time was longer than 3-sec, the target got off automatically. It is considered that the reaction time of pushing button became longer when the subjects got sleepy [21]. Because button was fixed on the steering wheel in this simulation, there was the possibility that button pushing task inflected driving task.

During driving simulation task, the cursor went straight when the subject didn't move the wheel. There were two situations led to the wheel stopped, one is the subject slept, the other occurred 4-sec before the subject reached the peak of sinusoidal lines until 4-sec after passing it. In the 8-sec portion, movement of wheel stopped along with the smoothness of road. Thus we defined the sleepiness was detected when stopping duration of wheel kept for more than 1-sec. Button was fixed on the steering wheel in this simulation, so there was the possibility that button pushing task inflected driving task. We rejected the wheel movement stopping event occurred 2-sec after pushing button event.

3.1.3 Qualification of the facial expression

We used a NTSC-DV (780×480, 0.9 pixel) with 30 frames per second to record facial expression of the subjects from face to chest. The qualification was made after the simulation. The facial expression was judged for every 4.5-sec epoch by monitoring the video images of the subject's face according to the criteria for sleepiness of rating (Table 3.1, [22, 23], written in Japanese with English summary).

Table 3.1: Facial expression sleepiness rating [22, 23]

0	**Not sleepy**	Roving eye movement, blink twice per second, involve the movement of body
1	**Slightly sleepy**	Opened mouth, slow glancing
2	**Sleepy**	High frequent slow eye blinking, mouth squirming, sit-up, touching face
3	**Rather sleepy**	Closing eyes tightly, moves body back and forth and around, yawns or enduring yawns, breathing deeply, slow eye blinks and slow glancing
4	**Very sleepy**	Closing eyes, bowed head, lifted up head
5	**Sleeping**	

3. 2 Electrophysiological recordings

3.2.1 Electroencephalography recordings

Electroencephalogram (EEG) was recorded (Multiamplifier-MA1132, Teac Corporation, Japan) from multiple electrodes placed on the cap (Ag/AgCI 32 channel Quik-cap, Neuroscan, USA) according to the International 10-20 system (Fig. 3.2) with sampling frequency at 500 Hz (DF－4B40－133 AD converter, Japan Think Net Corporation, Japan).

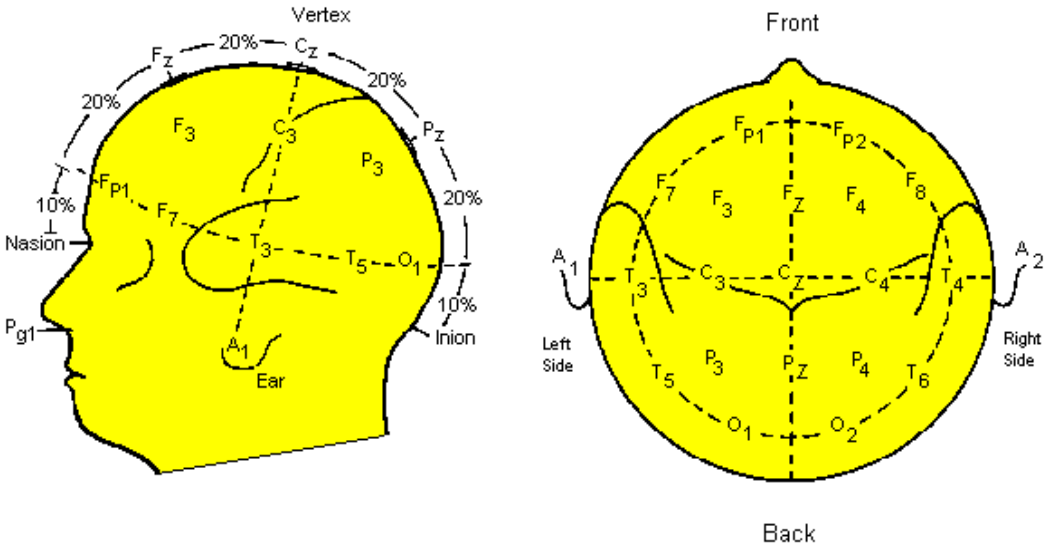

Figure 3.2 Side and top view of the international 10-20 system of electrode placement [26]

3.2.2 Electrooculogram recording

The electrooculogram (EOG) were recorded with pairs of electrodes placed above and below the right eye and to the left and right of the left eye [24]. Thus both vertical and horizontal movements of eyes were able to be monitored of the subject.

3.3 Artifacts Removal

Contamination of noise in EEG data frequently observed during the simulation. Most of the artifacts considered here are biological signals generated by sources external to the brain. Improving technology can decrease externally generated artifacts, such as line noise, but biological artifact signals must be removed after the recording process. For the accuracy of the following alpha rhythm analysis, removing the artifacts including eye movement, eye blink, muscle activity and blood pulse [25], especially the signals containing frequency component at alpha rhythm band, is necessary.

Because of its high amplitude an eye activity can corrupt data on all electrodes, even those at the back of the head. Eye artifacts are often measured more directly in the electrooculogram(EOG), pairs of electrodes placed above and around the eyes. Since the EOG are contaminated with EEG signals of interest, simple subtraction is not a removal option even if an exact model of EOG diffusion across the scalp is available [27].

Muscle activity including neck and facial muscles have a wide frequency range and can be distributed across different sets of electrodes depending on the location of source muscles. Muscle artifact contains activity at frequencies more than half the usual data acquisition rates for spectral EEG that may contribute power at conventional EEG frequencies by aliasing [28]. Brunner et al. reported short-lasting muscle artifacts in the sleep EEG more frequently towards the end of non-REM sleep periods [29, 31].

The blood pulse [28], or heart beat, artifact occurs when an electrode in placed on or near a blood vessel. The expansion and contraction of the vessel introduce voltage changes into the recording. The artifacts signal has a frequency component near 1 Hz, but can vary with the state of the patient. This artifact can appear as a sharp spike or smooth wave.

3.3.1 Source reparation by FastICA

We used FastICA based on Maximum Likelihood Estimation (MLE) to separate EEG signals and artifacts [34]. In the fixed-point algorithm for one unit, we had the following form of the FastICA algorithm [19]

$$w \leftarrow w - [E\{x(t)g(w^T x(t))\} + \beta w]/[E\{g'(w^T x(t)\} + \beta], \tag{3.1}$$

where $E\{\}$ is the average function. $\boldsymbol{x}$ is the observed signals and t indicates time. β can be computed as $\beta = -E\{\boldsymbol{y}(t)g(\boldsymbol{y}(t))\}$. Function $g(\cdot)$ is derivative of the non-quadratic function

$$\begin{aligned} g(x) &= \tanh(a_1 x) \\ g'(x) &= a_1(1 - \tanh^2(a_1 x)), \end{aligned} \tag{3.2}$$

where $1 \le a_1 \le 2$ is some suitable constant, often take as $a_1 = 1$.

For the matrix, the from is obtained as

$$\boldsymbol{W} \leftarrow \boldsymbol{W} + \boldsymbol{diag}(\alpha_i)[\boldsymbol{diag}(\beta_i) + E\{\boldsymbol{g}(\boldsymbol{y}_i(t))\boldsymbol{y}_i^T(t)\}]\boldsymbol{W}, \tag{3.3}$$

where β_i and α_i is defined as

$$\begin{aligned} \beta_i &= -E\{\boldsymbol{y}_i(t)g(\boldsymbol{y}_i(t))\} \\ \alpha_i &= -1/(E\{g'(\boldsymbol{w}_i^T \boldsymbol{x}_i(t)) + \beta_i\}), \end{aligned} \tag{3.4}$$

$\boldsymbol{diag}(\alpha_i)$ is a diagonal matrix with α_i on the *i-th* main diagonal.

3.3.2 Artifact identification

After the separation of recorded signals by FastICA, we got the ICs of recorded signals. We identified the artifacts by two steps: eye movement identification by calculating the cross-correlation coefficient between ICs and recorded EOG signals; muscle activity and pulse identification by power spectral density (PSD). After first two steps of the identification, we checked the sources of ICs by scalp topographic map.

Cross-correlation coefficient

We recorded eye movement during the driving simulation, so it is a simple way to find relationship between ICs and eye movement by the cross-correlation coefficient. The cross-correlation coefficient is a quantity that gives the quality of a least squares fitting to the original data. According to data, we set threshold for identify eye movement at 0.4. In the topographic map, the eye movement source is normally in the front of the scalp.

Power spectral analysis

The power spectral density (PSD) describes how the power of a time series is distributed with frequency. The muscle activities have a wide frequency range which is higher than EEG signals. So we used the PSD to identify the muscle activity from EEG signals. In the study, we focused on power of ICs at the 90-110 Hz frequency range. We considered IC as muscle activity if the power percentage larger than a threshold level.

PSD was estimated by using Welch's averaged modified periodogram method. The input IC was segmented into 480 sections of equal length, each with 50% overlap. Each segment was windowed with a Hamming window that is same length as the segment [39].

Scalp topographic map

Topographic map is one way to present EEG information. It can obviously be used for the approximation of the cortical potential. In the topographic map, the scalp potential distribution reflects the distribution of intracranial electrical sources and fields. The potentials at a certain moment or period of time are coded as colors at the corresponding electrode locations. The electrical potential values on spaces between the electrode points are linearly interpolated [30]. In this study, we used a simple way to present the scalp by spherical sketch of the head as a cranial projection and approximated the electrical potential values on spaces between the electrode points by inverse distance method [37]. According to the scalp topographic map, we can confirm the category of artifacts.

3.4 Analysis methods

3.4.1 Wavelet analysis

After the artifact removal of EEG recordings, continuous wavelet analysis was conducted to detect alpha wave component from EEG. The wavelet transform yielded a complex-valued spectral temporal representation for each electrode signal. Wavelet transform is a method to analyze signals in time for its frequency content. We can get the wavelet coefficients in complex-valued as following:

$$T(a,b) = \frac{1}{\sqrt{a}} \int_{-\infty}^{\infty} x(t) \psi^{*}\left(\frac{t-b}{a}\right) dt \qquad (3.5)$$

where a and b indicate the scale and shift respectively. $\psi(t)$ is the mother wavelet function, * means the complex conjugate.

In this study, we used the complex Morlet wavelet as mother wavelet.

(3.6)

$$\psi(t) = \frac{1}{\pi^{1/4}} \exp(i2\pi f_c t) \exp\left(-t^2 / f_b\right) \tag{3.7}$$

where, $f_b (= 2)$ and $f_c (= 0.894)$ are bandwidth parameter and wavelet center frequency, respectively.

3.4.2 Alpha rhythm extraction

In order to investigate the relationship between EEG alpha rhythm and sleepiness, we conducted extraction of alpha rhythm after the artifacts removal (Figure 3.3). We used band-pass filter (pass-band 8-13 Hz) and wavelet analysis. The complex-valued alpha rhythm was given by wavelet analysis.

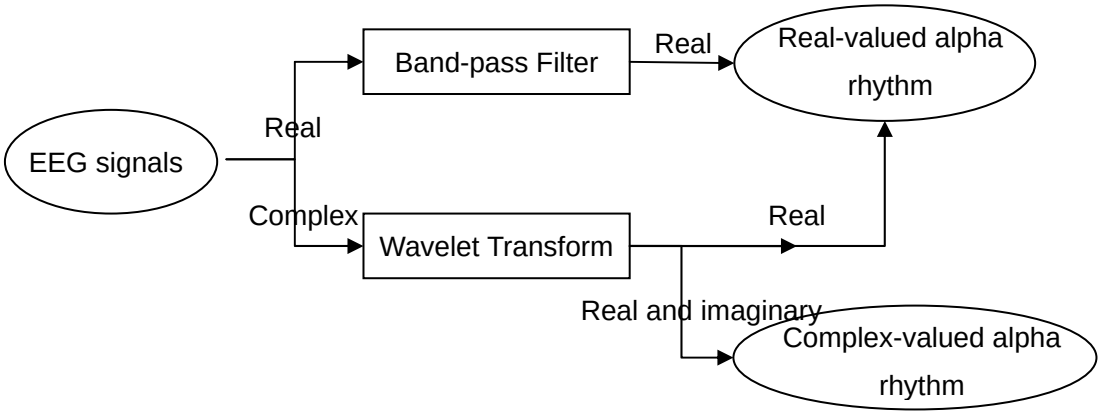

Figure 3.3 Schematic representation of the processing stages of the alpha rhythm extraction in real-valued analysis and complex-valued analysis.

3.4.3 Alpha rhythm detection

Alpha rhythm was detected as rhythmic activity (8-13 Hz) whose absolute value of wavelet coefficient (8-13 Hz, depending on the subject) was larger than the threshold level for more than 500-ms (Figure 3.4). The threshold level was set to the m+5sd, where m is mean and sd is standard deviation for the first 5-min of the data (no alpha rhythm is included). Alpha rhythm was considered to exist even detected in only one channel. The time epochs containing alpha rhythm component were gathered for the following analysis.

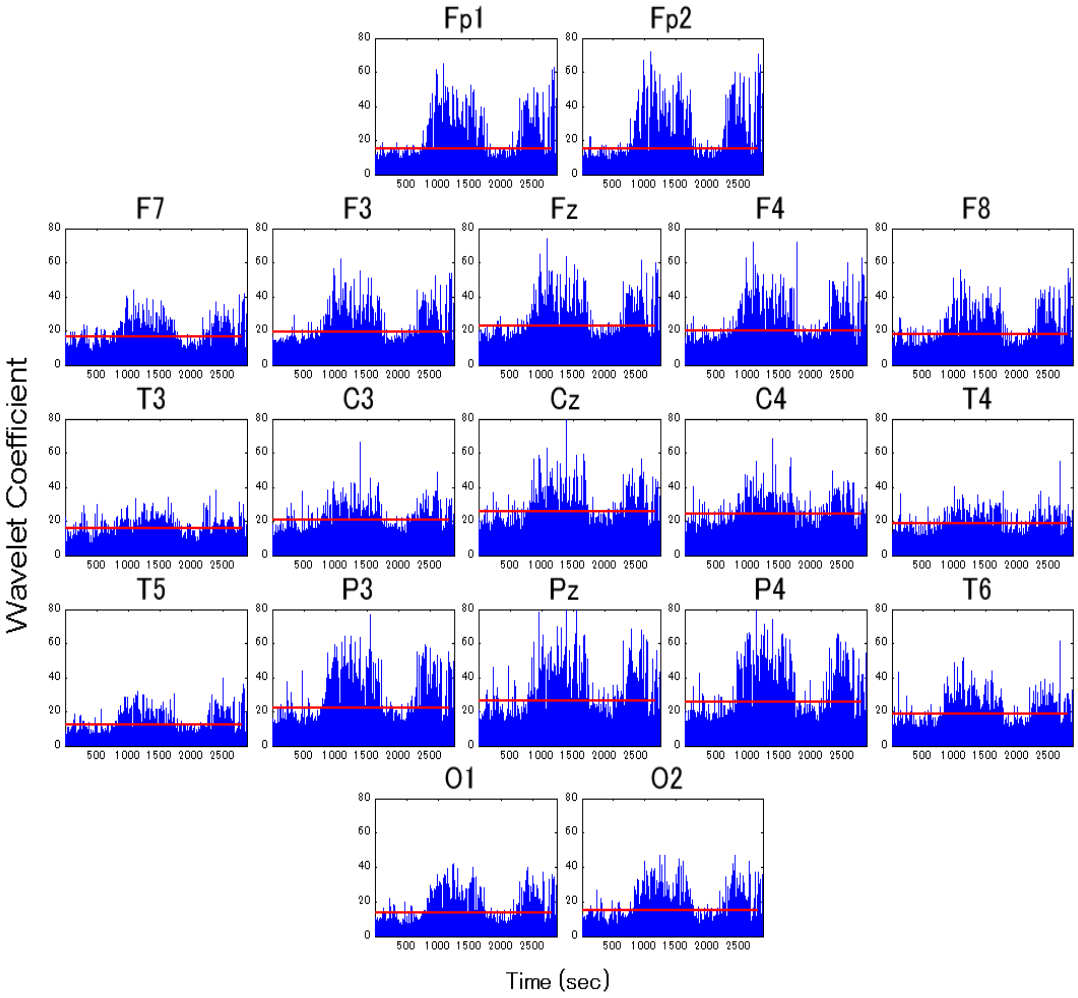

Figure 3.4 Time evaluation of alpha rhythm power of 19 channels Blue (Subject 1). Red line indicates the threshold level for the channel.

3.4.4 Principal Component Analysis (PCA)

After the detection of alpha rhythm, we applied real-valued and complex-valued PCA to reduce the dimension of signals (Figure 3.5). PCA involves a mathematical procedure that transforms a number of possibly correlated variables into a smaller number of uncorrelated variables called principal components.

In mathematical terms, consider a linear model as follows [19]

$$\boldsymbol{y}_1(t) = \sum_{k=1}^{n} w_{k1} x_k(t) = \boldsymbol{w}_1^T \boldsymbol{x}(t), \tag{3.8}$$

where $x_i(t)$ is a vector of the observed signals $\boldsymbol{x}(t)$. The $w_{11},\ldots,w_{n1}$ are scalar coefficients, elements of an n-dimensional vector of $\boldsymbol{w}_1$, and T denotes the transpose. The factor $\boldsymbol{y}_1$ is

called the first principal component of $\boldsymbol{x}$, if the variance of $\boldsymbol{y}_1$ is maximally large. The first principal component accounts for as much of the variability in the data as possible, and each succeeding component accounts for as much of the remaining variability as possible. Thus we look for weight vector maximizing the PCA criterion

$$E\{\boldsymbol{y}_1^2(t)\} = E\{(\boldsymbol{w}_1^T\boldsymbol{x}(t))^2\} = \boldsymbol{w}_1^T E\{\boldsymbol{x}(t)\boldsymbol{x}^T(t)\}\boldsymbol{w}_1 = \boldsymbol{w}_1^T\boldsymbol{C}_x\boldsymbol{w}_1, \tag{3.9}$$

where $E\{\cdot\}$ is the expectation over the density of input vector $\boldsymbol{x}(t)$, the matrix $\boldsymbol{C}_x$ is the covariance matrix of $\boldsymbol{x}$ given for the zero-mean vector x by the correlation matrix

$$\boldsymbol{C}_x = E\{\boldsymbol{x}(t)\boldsymbol{x}^T(t)\}. \tag{3.10}$$

The solution to the PCA problem is given in terms of the unit-length eigenvectors $\boldsymbol{e}_1,\ldots,\boldsymbol{e}_n$ of the matrix $\boldsymbol{C}_x$. The ordering of the eigenvectors is such that the corresponding eigenvalues $d_1,\ldots,d_n$ satisfy $d_1 > d_2 > \ldots > d_n$. The solution is given by

$$\boldsymbol{w}_1 = \boldsymbol{e}_1.$$

Thus the first principal component of $\boldsymbol{x}$ is $\boldsymbol{y}_1 = \boldsymbol{e}_1^T\boldsymbol{x}(t)$. The criterion also can be generalized to m principal components.

Figure 3.5 showed the results by real-valued and complex-valued PCA. According to cumulative contribution, it is suggested that first PC was more concentrated in complex-valued analysis than real-valued analysis when the phase shift existed obviously.

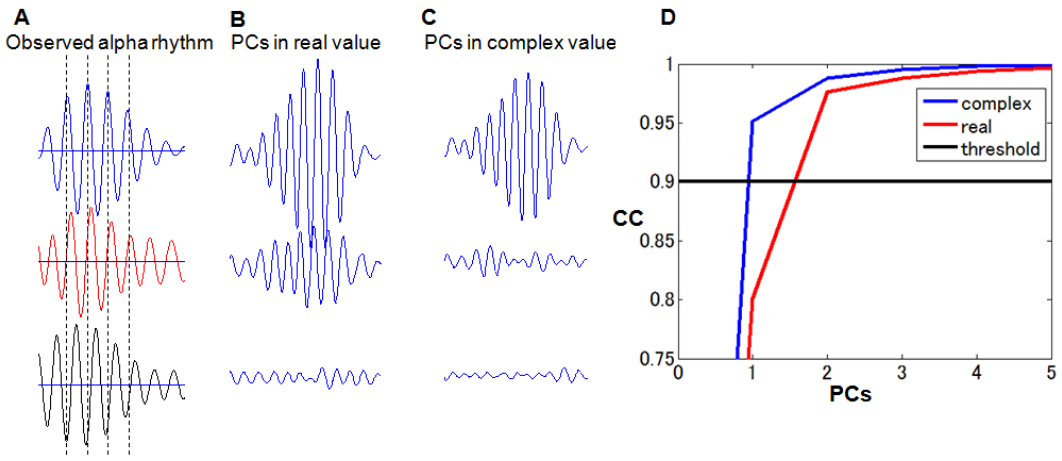

Figure 3.5 Results of PCA in real-valued and complex-valued analysis. A: observed alpha rhythm in which phase shift exists between either two of three channels. B: first three PCs in real-valued. C: first three PCs in complex-valued. D: cumulative contribution of PCs. CC: cumulative contribution. Blue: result in complex-valued PCA. Red: result in real-valued PCA. Black: 90%

which is the threshold for explaining data well enough.

3.4.5 Complex-valued ICA

If the mixing process is not instantaneous, i.e., the observed signal $\boldsymbol{x}$ is a mixture of delayed source signal $\boldsymbol{s}$, the linear mixing model is described by the following equation:

$$\mathbf{x}(t) = \mathbf{A} * \mathbf{s}(t), \tag{3.11}$$

where t is time, $\mathbf{A}$ is an impulse response matrix (from sources to recording channels) and * is convolution operator. In this study, we assume that the following relation is approximately satisfied:

$$\hat{\mathbf{x}}(\omega,t) \approx \hat{\mathbf{A}}(\omega)\hat{\mathbf{s}}(\omega,t), \tag{3.12}$$

where ω is frequency, $\hat{\mathbf{A}}(\omega)$ is Fourier transform of $\mathbf{A}$. $\hat{\mathbf{x}}(\omega,t)$ and $\hat{\mathbf{s}}(\omega,t)$ are time-frequency domain representation of $\mathbf{x}(t)$ and $\mathbf{s}(t)$, respectively; thereby, they are complex-valued functions. Note that the convolutive mixture is transformed into instantaneous mixture. Therefore, estimation of the source signal $\hat{\mathbf{y}}(\omega,t)$ would be given as follows:

$$\hat{\mathbf{y}}(\omega,t) = \mathbf{W}(\omega)\hat{\mathbf{x}}(\omega,t) \tag{3.13}$$

where $\mathbf{W}(\omega)$ is an unmixing matrix whose elements are complex numbers. In this study, $\hat{\mathbf{x}}(\omega,t)$ is obtained by continuous wavelet transform (complex number vector of wavelet coefficients corresponding to alpha wave activity). $\mathbf{W}(\omega)$ was estimated by using natural gradient maximum likelihood algorithm for complex-valued signals as follow [35,36]

$$\begin{aligned} \Delta W &= -\mu[I - g^*(y, y^*)y^H]W \\ g(y, y^*) &= \tanh(|y|)e^{-j\theta(y)} \end{aligned}, \tag{3.14}$$

Before applying complex-valued ICA, the complex-valued vector was whitened by using principle component analysis. In addition, the dimensionality of the vector was reduced to 3-5 (dependent on the subject) and assumed complete condition (i.e. $m = n$).

3.4.6 Degree of separation

To quantify the degree of separation achieved by the real-valued and complex-valued ICA algorithms, we computed residual statistical dependencies using fourth order statistics described [38].

Fourth order statistical dependencies were taken into account by computing, for different estimated number of ICs (=*N*), the mean $\rho(N)$ of the absolute values of cross-cumulant $\rho_{ij}(N)$ for all different component pairs $i \neq j$:

$$\rho(N) = \frac{1}{N(N-1)} \sum_{i \neq j} \rho_{ij}(N), \tag{3.15}$$

where the cross-cumulant were defined as

$$\rho_{ij}(N) = \left| \frac{E\{|y_i(\omega,t)|^2 |y_j(\omega,t)|^2\} - \mu_i(N)\mu_j(N)}{\sigma_i(N)\sigma_j(N)} \right|, \tag{3.16}$$

$$\mu_i(N) = E\{|y_i(\omega,t)|^2\}, \tag{3.17}$$

$$\sigma_i(N) = \sqrt{E\{(|y_i(\omega,t)|^2 - \mu_i(\omega,t))^2\}}. \tag{3.18}$$

The value of $\rho_{ij}(N)$ is zero for independent signals, non-zero for signals exhibiting correlated fluctuations in signal power, and 1 only for signals with proportional squared-amplitude time-courses.

3.4.7 Topographic analysis of alpha sources

The independent components extracted by ICA were supposed to be the source of alpha wave of EEG. To display topographic profile of each source, reverse process of extracting ICs was conducted. For example, projection of the second independent component $\mathbf{c}_2 = [0,1,0,\ldots,0]^T$ onto the recording channels $\mathbf{z}_2$ is calculated as follows:

$$\mathbf{z}_2 = \mathbf{V}^{-1}\mathbf{W}^{-1}\mathbf{c}_2, \tag{3.19}$$

where $\mathbf{W}$ is the unmixing matrix and $\mathbf{V}$ is the whitening matrix.

Figure 3.6 shows the procedure from which we got one of ICs time-series waveform projecting in original 19 electrodes. The interpolation method [37] for the point between the positions of 19 electrodes was shown as follow:

$$w(x) = \sum_{j=1}^{19} \alpha_j \phi_2(x - x_j), \tag{3.20}$$

where x is the position in the 2-dimensional space. α_j is found by solving the linear system

$$w_i = \sum_{j=1}^{19} \alpha_j \phi_2(x_i - x_j) \quad , \qquad (3.21)$$
$$\phi_2(x) = |x|^2(\ln|x| - 1)$$

where $\phi_2(x)$ is the biharmonic Green Function in 2-demensions.

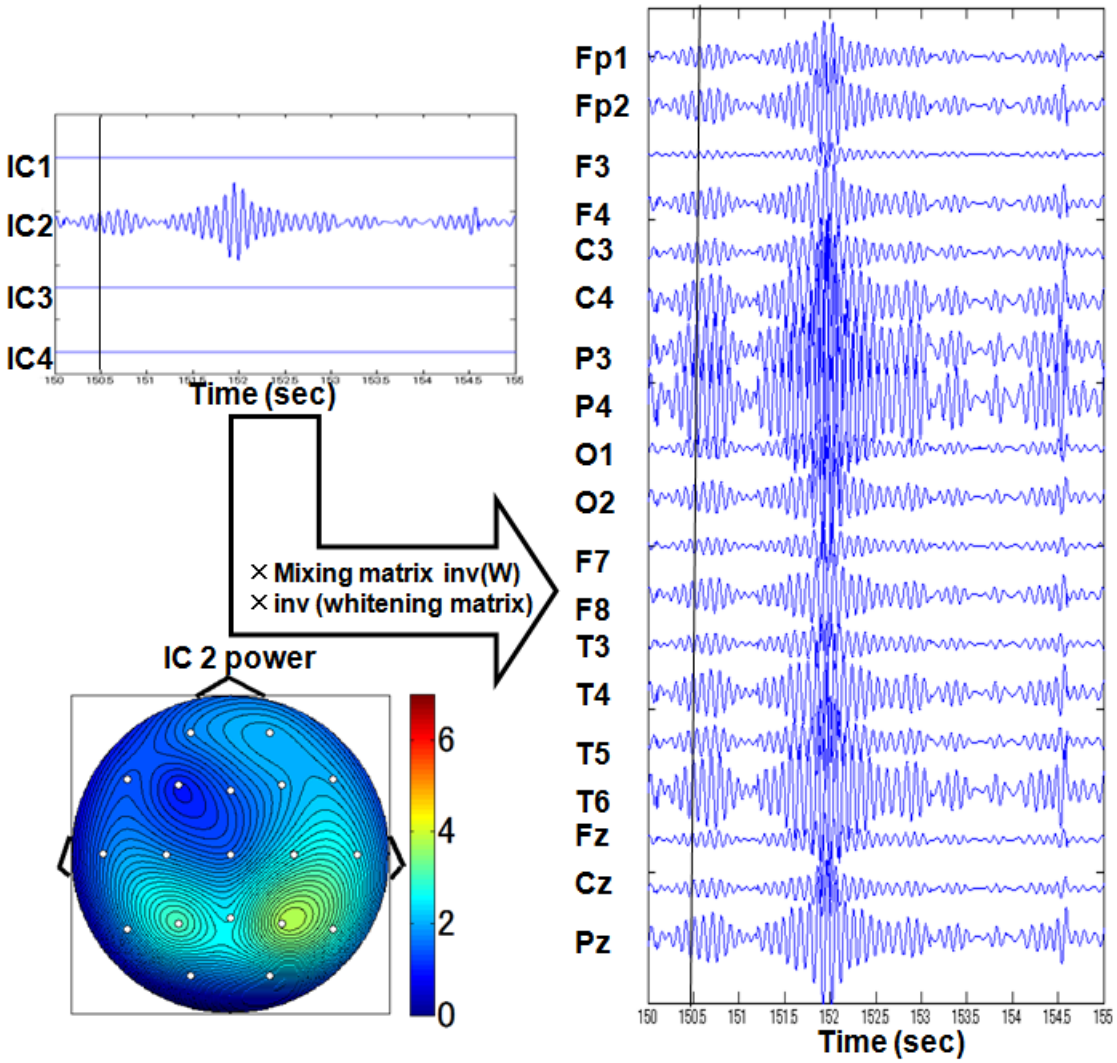

Figure 3.6 Projection of the selected IC.

Chapter 4 Results and discussion

4.1 Characteristic of recorded signals

4.1.1 Performance

Figure 4.1 shows a 25-sec portion (one cycle) of the driving track during a driving simulation task. It is shown that the cursor began to deviate from the road at 1475-sec, suggesting the subject just got sleep. At the same time, difference between road center and cursor began to increase (Figure 4.1C). At about 2-sec after the onset of stopping moving, the subject was supposed to get wakeful again, and tried to correct the direction of cursor. Difference got smaller, and paroxysmal movement took place. In the facial expression, the level also got lower simultaneously. In this task, we considered the time when subject stopped moving wheel was the onset of sleepiness.

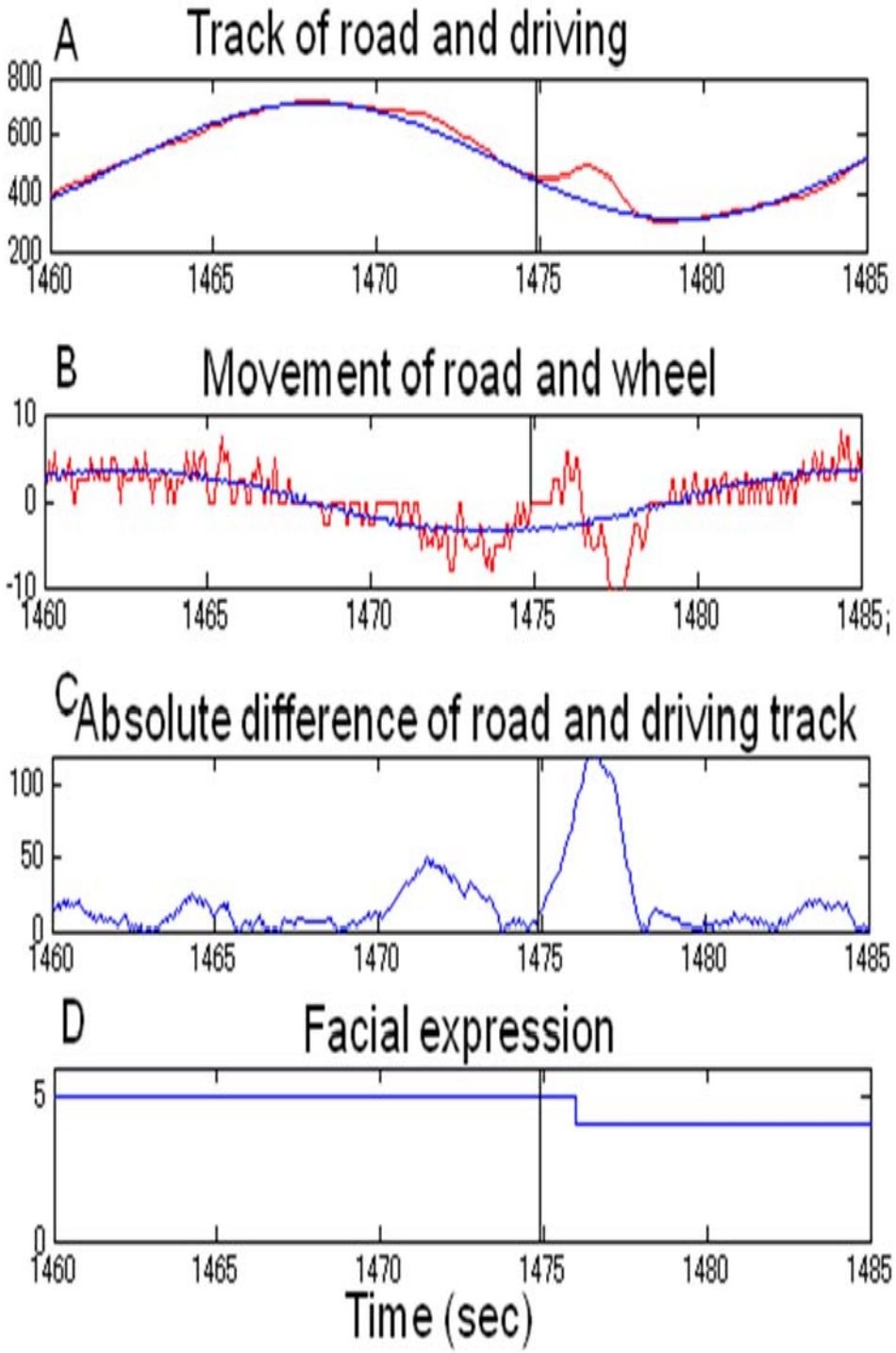

Figure 4.1 Driving performances in one cycle. A: track of road and driving (blue: road, red: driving track). B: movement of road and wheel (blue: road, red: wheel). C: difference between road centre and driving track. D: Facial expression.

Figure 4.2 shows the reaction time in response to flash stimulation during the simulation. The performance was evaluated in terms of the duration of the reaction time, i.e., i: no pushing, ii: reaction time is longer than 1.5-sec, iii: reaction time is shorter than 1.5-sec longer than 0.8-sec, iv: reaction time is shorter than 0.8-sec. [26]

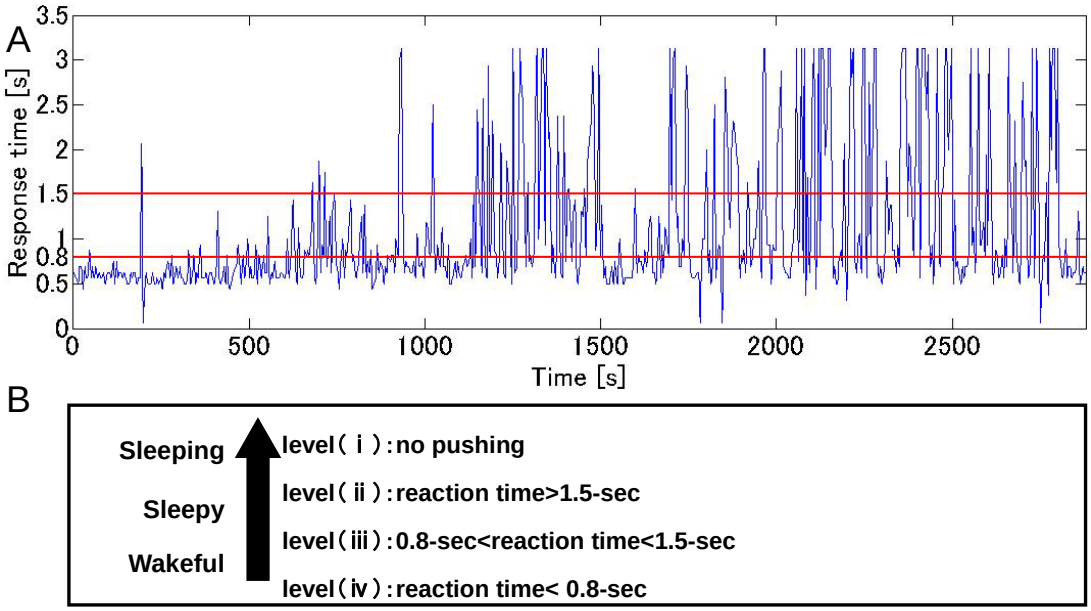

Figure 4.2 Sleepiness level according to the reaction time. A: reaction time during the simulation. Red lines indicate the threshold which judges the level of sleepiness. B: principal of sleepiness level division. We assumed the longer reaction time, the sleepier of the subject.

4.1.2 EEG and EOG

Figure 4.3 shows waveforms of 10-sec portion of the EEG and EOG. In the figure, EOG with high amplitude corrupts signals on most of EEG electrodes, even those at the back of the head. Muscle activity with higher frequency component than EEG signals were observed on all of the electrodes near 2046-sec.

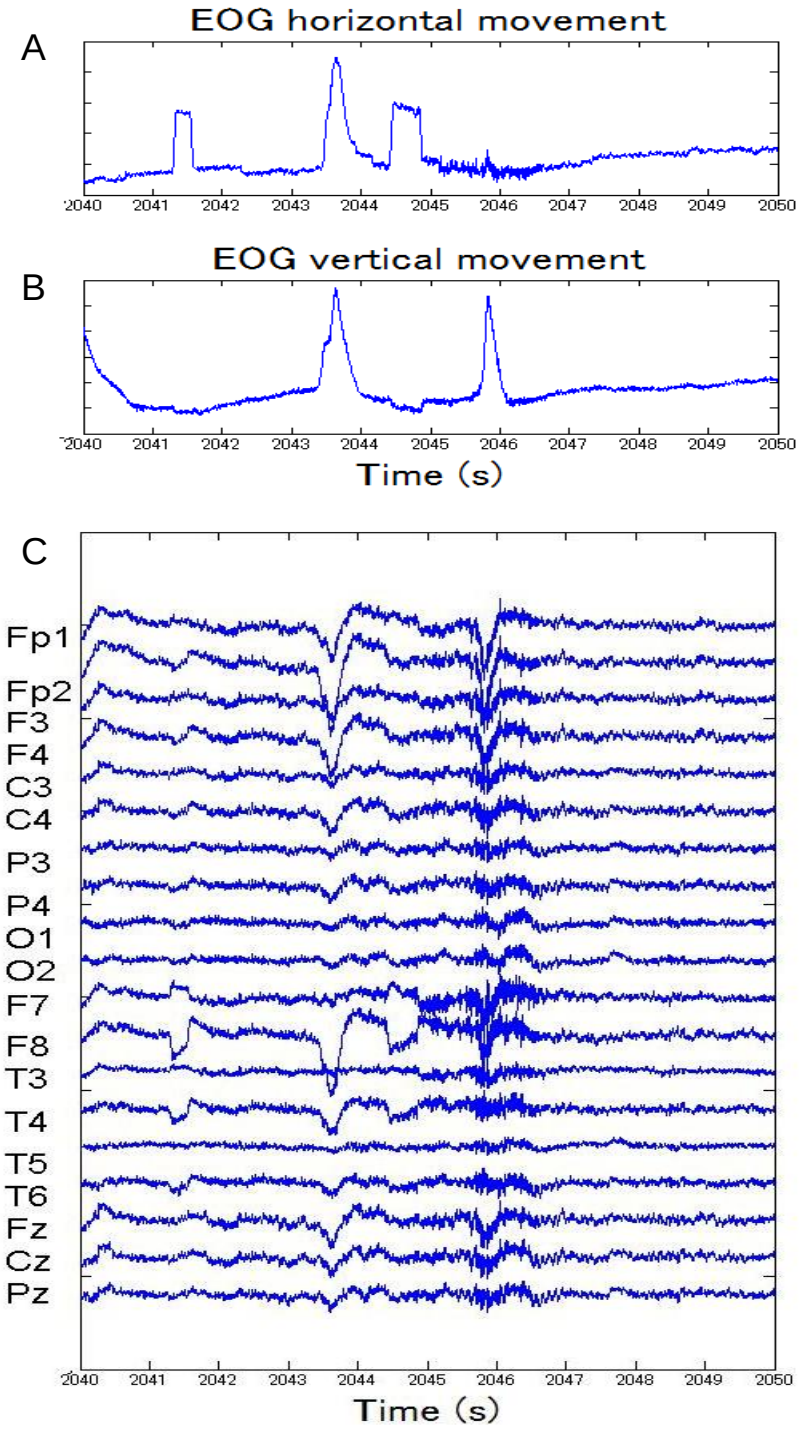

Figure 4.3 Waveforms of EOG and EEG in 10-sec portion. A: eye horizontal movement, B: eye vertical movement, C: 19 channels recoded signals.

4.2 Artifacts removal

Figure 4.4 shows relationship between ICs and eye movement. Bar graph shows correlation coefficient (Figure 4.4A). In this subject we found two ICs have significantly higher correlation with EOG. Scatter diagram of the ICs and EOG also shows significant correlation. In addition, the topographic maps of the sources concentrated in the facial area. The source of eye horizontal movement (IC17) is at frontal temporal site, while eye vertical movement (IC14) is at frontal polar site. These results suggest that the ICs 14 and 17 correspond eye movement potentials.

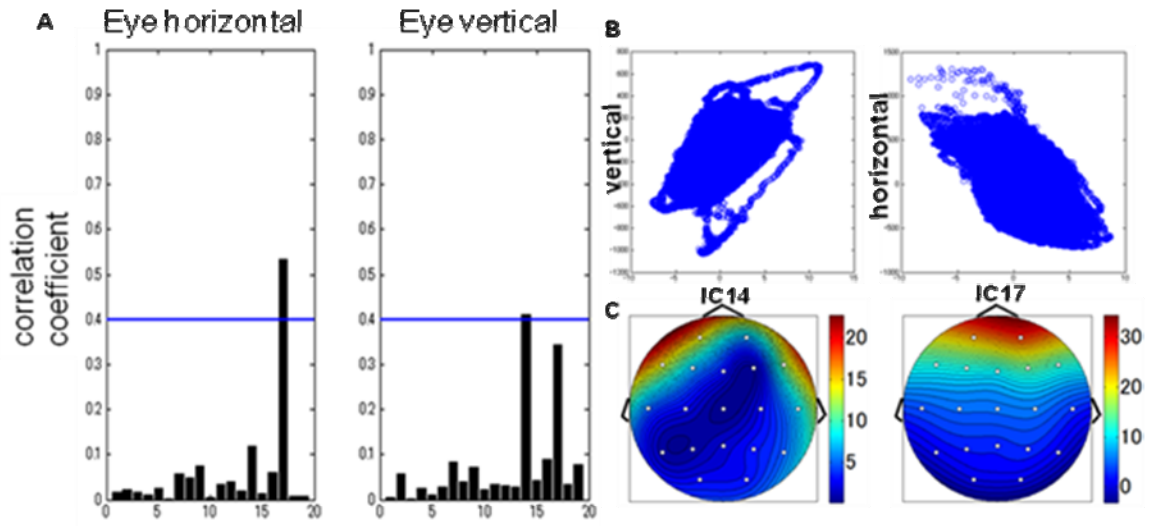

Figure 4.4 Relationship between ICs and eye movement. A: Correlation coefficient between ICs and eye horizontal (left histogram) and vertical (right histogram) movement. Horizontal blue line is the threshold. B: Significant correlations of two ICs with highest association, eye movement. C: Topographic map of selected two ICs.

In Figure 4.5, the power spectral density results of selected two ICs (IC12 and 15) are shown. PSD of IC15 in the frequency near 100Hz which is dominant frequency band of muscle activity is much higher than IC12. In Figure 4.5, PSD at 60 and 120 Hz (integral multiple of the A/C frequency in Nagoya where we made the simulation) could be observed. In order to reject the influence of line noise, we calculated the power percentage in 90-110 Hz to identify the artifacts of muscle activity.

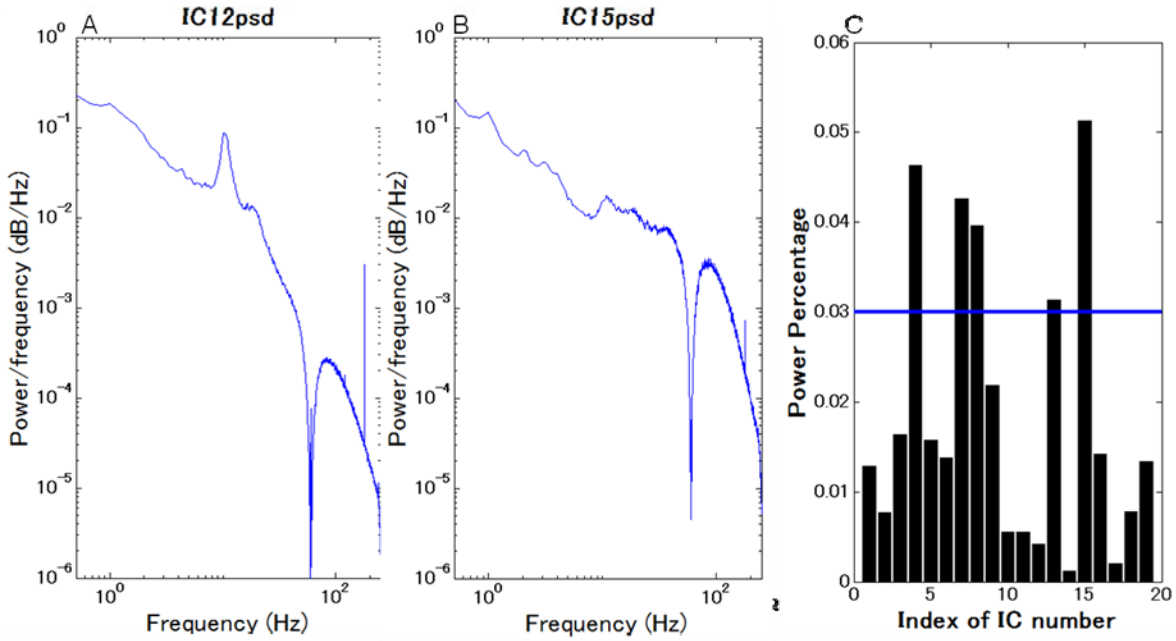

Figure 4.5 PSD of ICs. A: PSD of IC12 (EEG signal). B: PSD of IC15 (muscle activity). C: Power percentage in 90-110 Hz (red: threshold for identifying muscle activity)

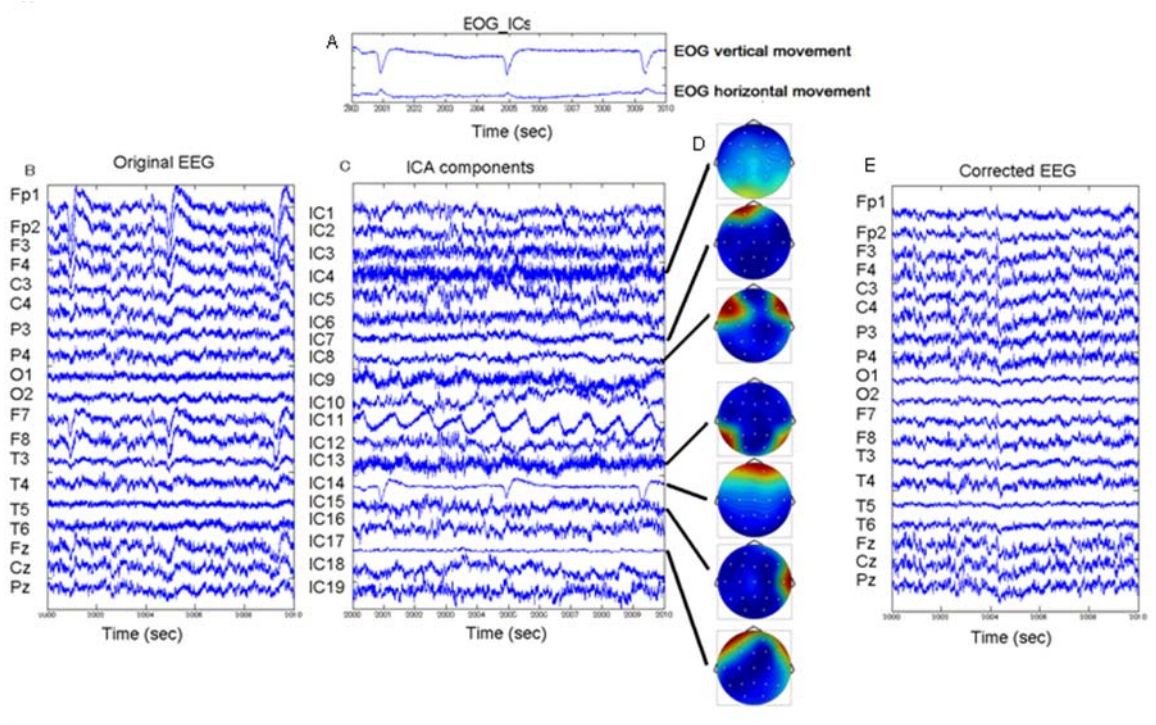

Figure 4.6 Artifacts removal by using ICA. A 10-sec portion of EOG time series (A), corresponding EEG time series (B), independent components (C) with scalp power map of 7 selected ICs (D) and corrected EEG (E). These data were collected from Subject 1.

Figure 4.6 shows a 10-sec portion of the EOG signals (A), corresponding original EEG time series (B), independent components (ICs) estimated by FastICA (C), scalp topography of 7 selected components (D) and the corrected EEG signals (E) obtained by removing the 7 selected components from the original data. The reasons to remove these ICs are as follows: (1) the waveforms of ICs 14 and 17 were quite similar to that of eye movement potentials (EOG). The scalp maps indicate that spread of these components agrees well with that of EOG. They have a linear relationship with eye movement. (2) ICs 4, 7, 8, 13 and 15 mainly contain very high-frequency component. According to the scalp maps, ICs 4 and 13 are found in the occipital region. In the region, the muscle potentials associated with the neck movement can easily contaminate to the EEG. ICs 7 and 8 are found in the frontal region. In the region, the potentials associated with the face muscle activity can easily contaminate to the EEG. IC15 is found right temporal which is associated with the ear muscle activity. Thereby, these ICs are suggested to be electromyograms. (3) In addition, there is a periodic component (IC11). Since the frequency is near 1 Hz as the human's heart rate, we judged the IC represents cardiac

artifact. As a result, we got the corrected EEG data which is almost free from the artifacts.

The performance of artifacts rejection of other subjects (Subject2, 5, 6, 9) was shown in Figure 4.7~4.10. In the other subjects, the eye vertical movement was separated successfully. Some of the muscle activities generated by neck or face were also separated. The corrected EEG signals after the selected artifacts removal were more free than the original EEG signals.

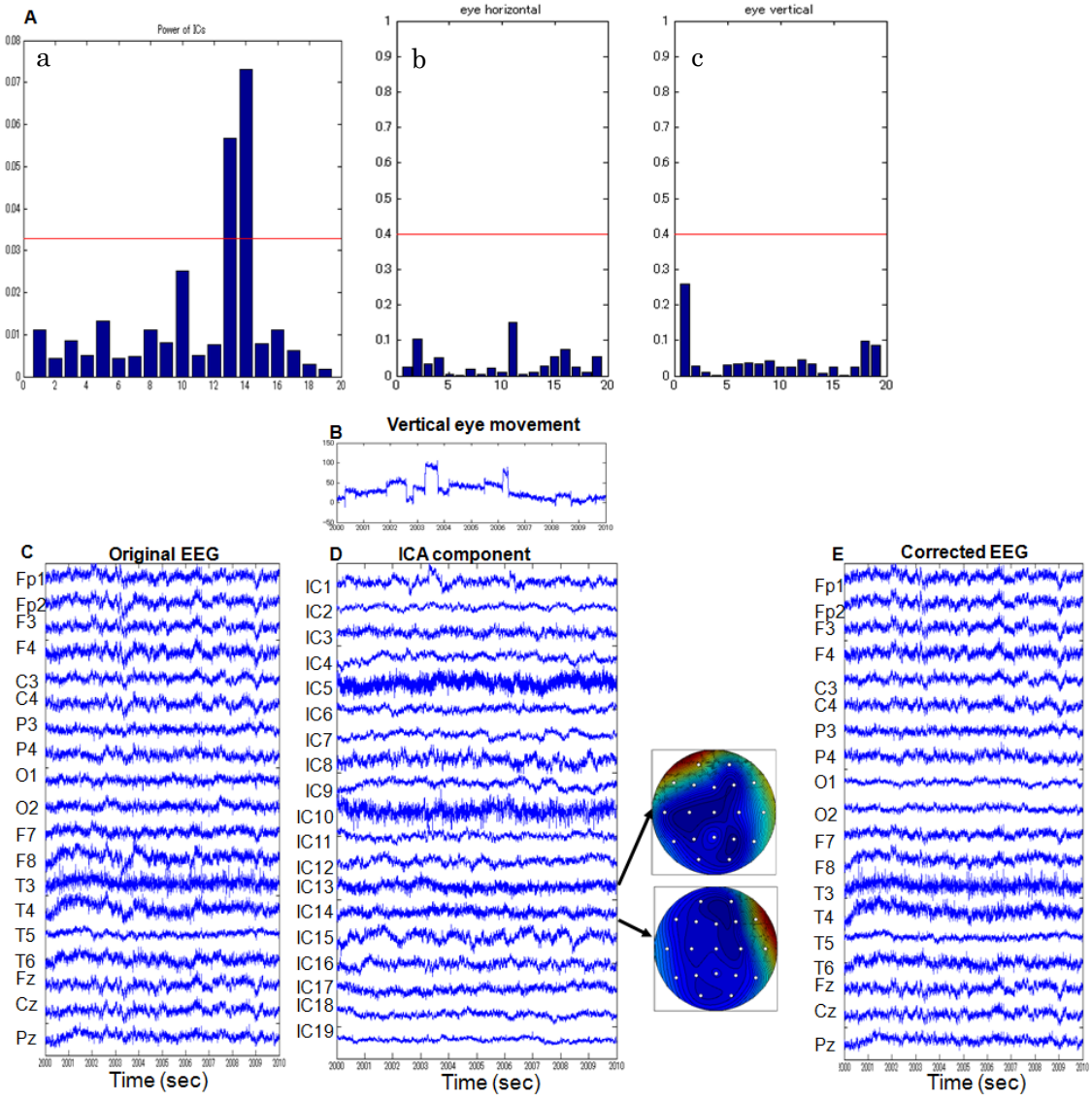

Figure 4.7 The artifacts removal result of Subject 2. Power percentage in 90-110 Hz for each IC, correlation coefficient between ICs and eye movement (A), a 10-sec EOG vertical movement (B), corresponding EEG time series (C), independent components (ICs) with scalp power map of 2 selected ICs (D) and corrected EEG (E).

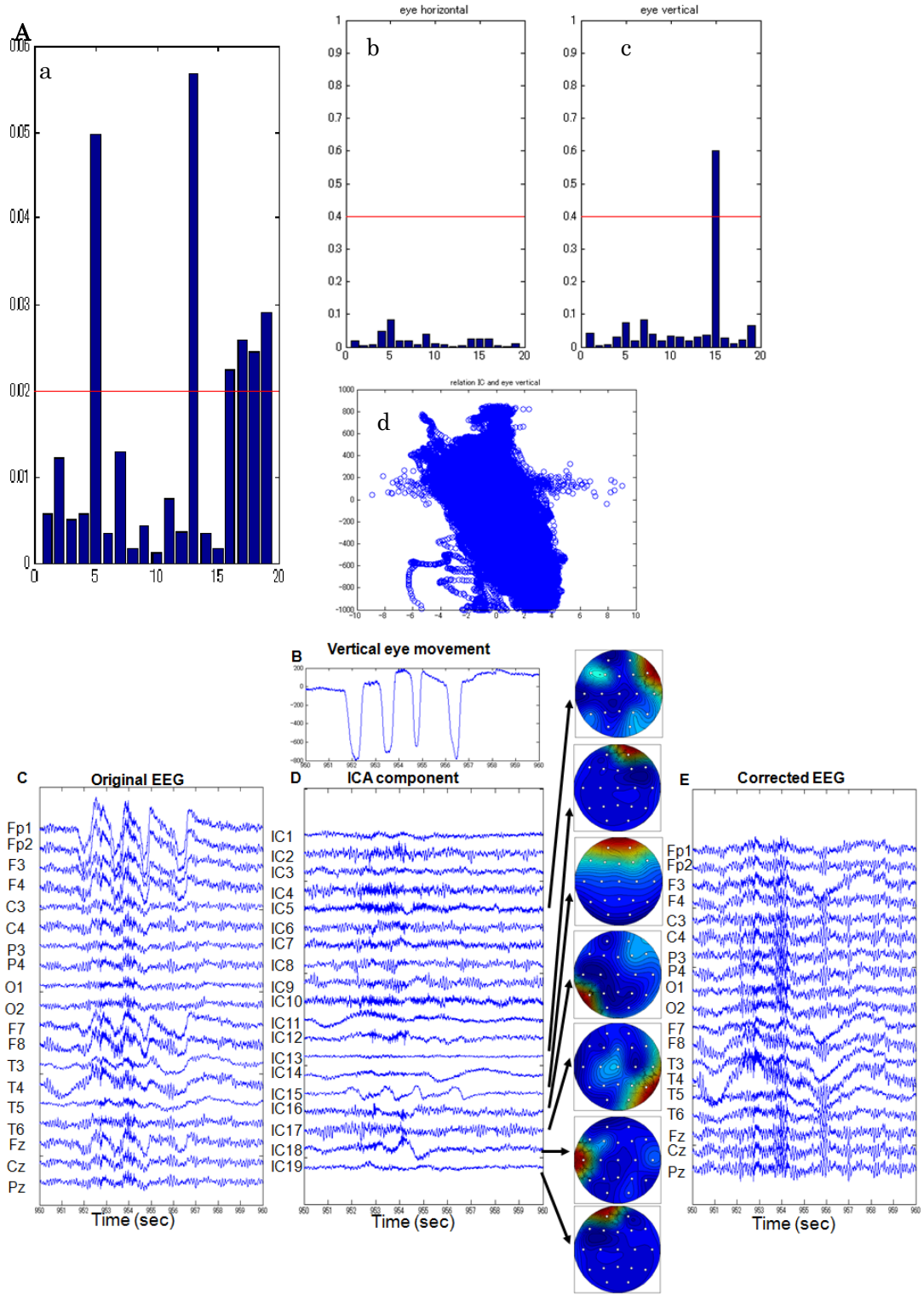

Figure 4.8 The artifacts removal result of Subject 5. Power percentage in 90-110 Hz for each IC, correlation coefficient between ICs and eye movement (A), a 10-sec EOG vertical movement (B), corresponding EEG time series (C), independent components (ICs) with scalp power map of 3 selected ICs (D) and corrected EEG (E).

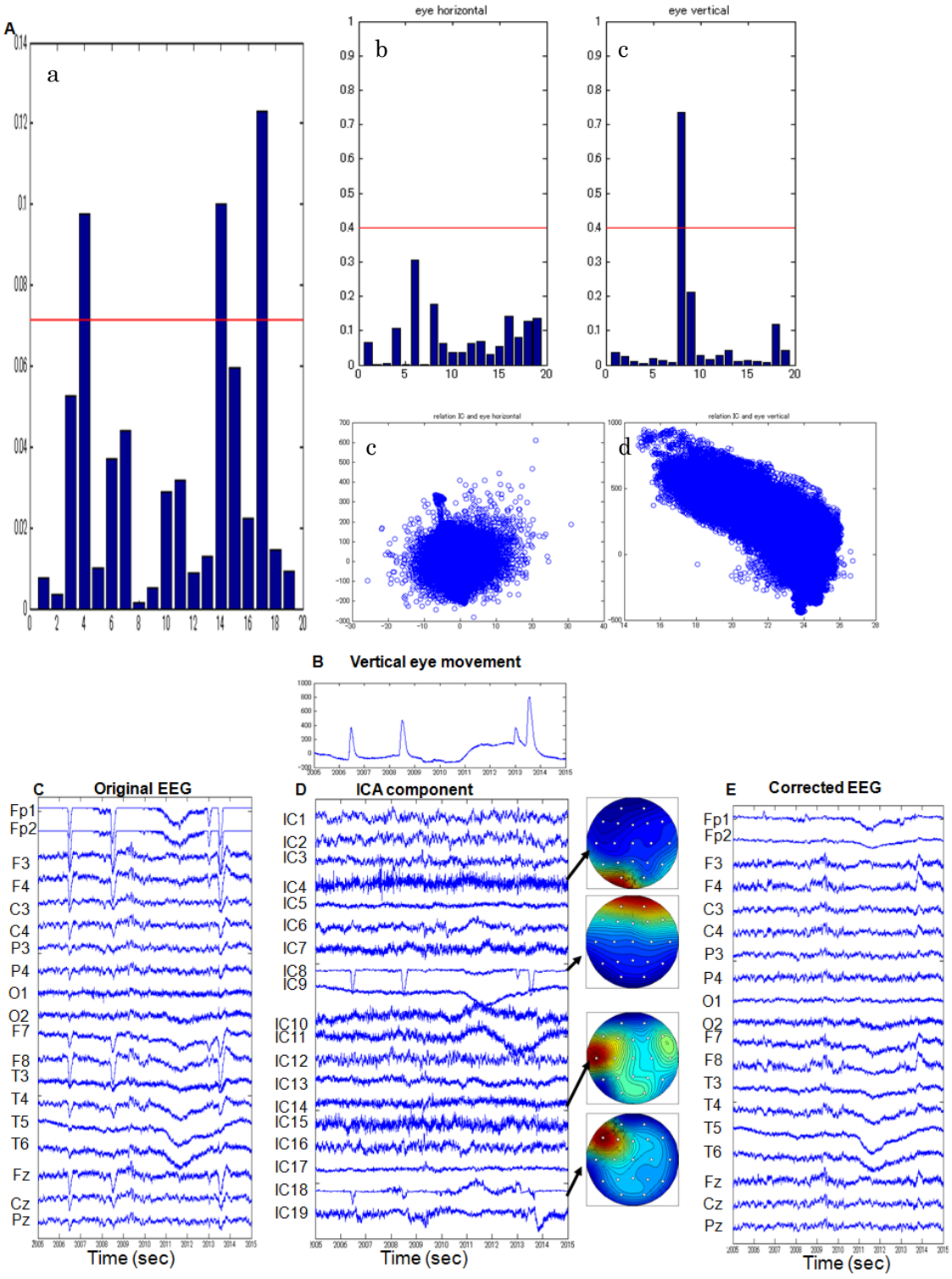

Figure 4.9 The artifacts removal result of Subject 6. Power percentage in 90-110 Hz for each IC, correlation coefficient between ICs and eye movement (A), a 10-sec EOG vertical movement (B), corresponding EEG time series (C), independent components (ICs) with scalp power map of 4 selected ICs (D) and corrected EEG (E).

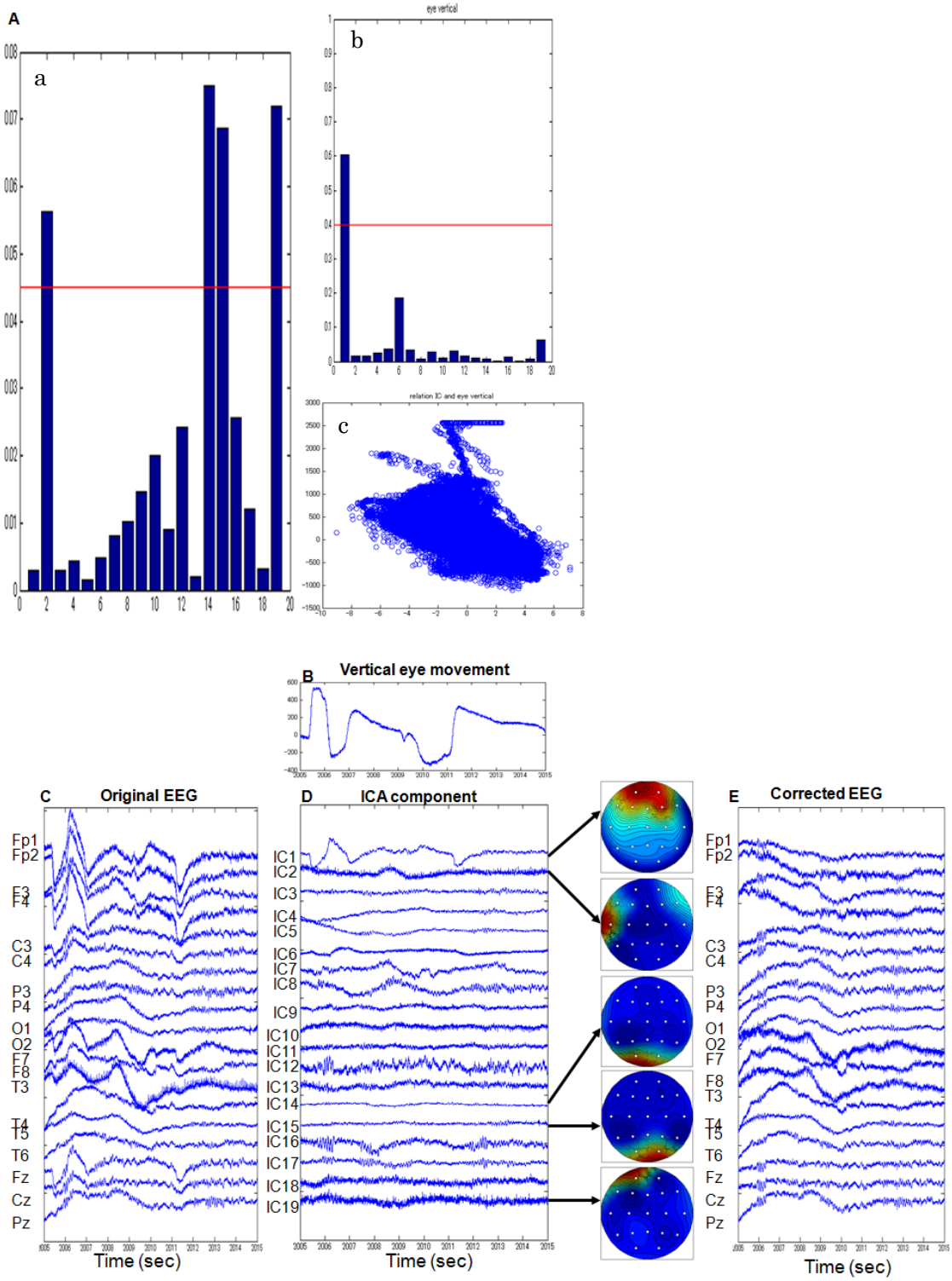

Figure 4.10 The artifacts removal result of Subject 9. Power percentage in 90-110 Hz for each IC, correlation coefficient between ICs and eye movement (A), a 10-sec EOG vertical movement (B), corresponding EEG time series (C), independent components (ICs) with scalp power map of 5 selected ICs (D) and corrected EEG (E).

We proved the improvement after the artifacts rejection by the other method. We separated the original EEG signals and corrected EEG signals by the same method. If the sources of original EEG signals have obvious eye movement or muscle activity components which are not observed in the corrected EEG signals, the improvement by the artifacts rejection can be proved. As shown in Figure 4, the number of ICs (Subject 6) without artifacts removal is larger than result with artifacts removal. It is obvious that eye movement (IC1) was observed in the separated sources. On the other hand, the component of occipital alpha rhythms could not be extracted from the original EEG signals. Therefore, we conclude that the artifacts removal procedure improves the accuracy of source decomposition of alpha EEG.

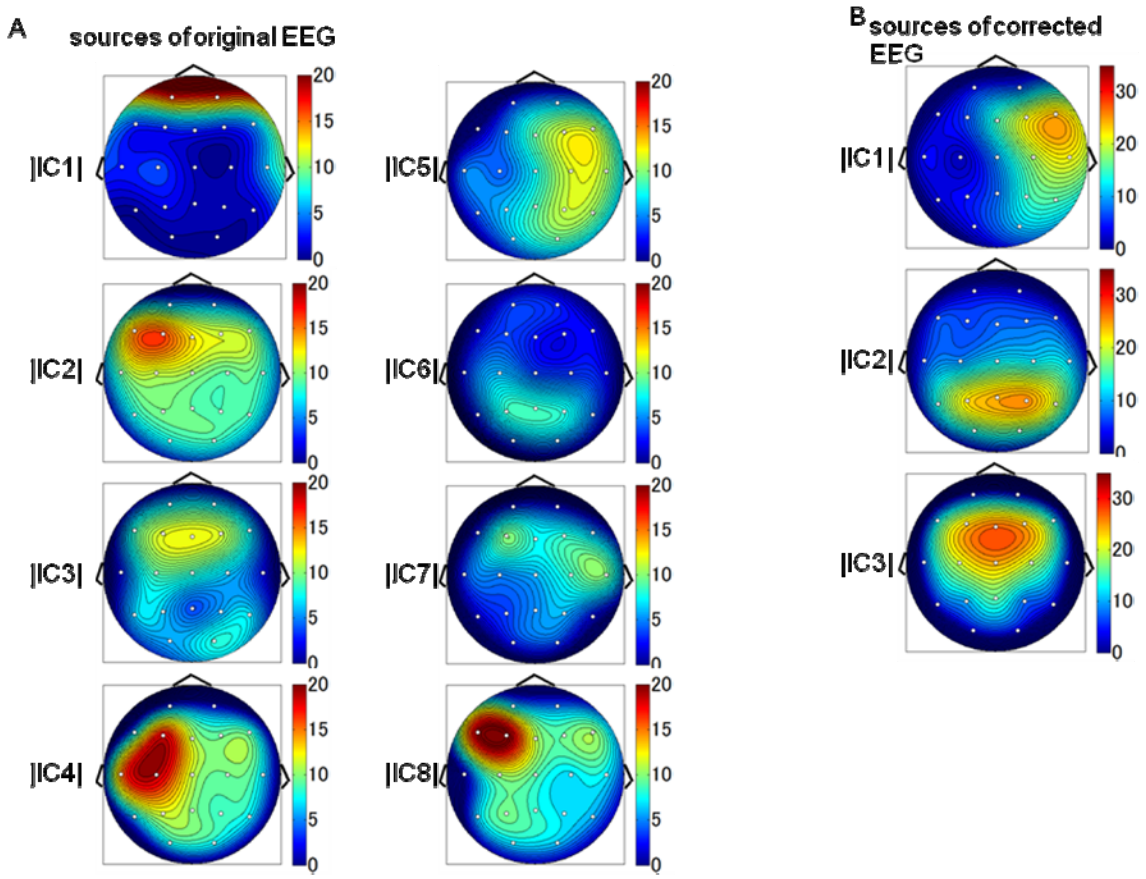

Figure 4.11 Comparison of sources of original EEG signals (A) and corrected EEG (B) signals (Subject 6).

4.3 Comparison of real-valued and complex-valued ICA

To decompose the source of EEG alpha rhythms, ICA was applied to the alpha band component of EEG, which was obtained by using band-pass filter (pass-band 8-13 Hz) or wavelet analysis (center frequency 10 Hz).

In the case of the Subject 1 presented here, the dimension of alpha EEG signals was reduced from nineteen to four; as a result, four ICs were obtained by ICA. The decomposed ICs are sorted according to the similarity of their power topographic maps to make comparisons easier.

Figure 4.12 A and B show the power maps of alpha ICs obtained by real-valued ICA. As shown, the real-valued ICA provides the similar maps despite the preprocessing method. Figure 4.12 C shows the topography maps of alpha ICs obtained by the combination of complex-valued wavelet analysis and complex-valued ICA. In this case, the map has information about both amplitude (power) and phase difference between recording sites. On the power maps, IC 2, 3 and 4 are similar to those obtained by real-valued ICA. On the phase maps of ICs 2, 3 and 4, the phase shift was observed obviously along the surface of scalp, and is almost reversed from the frontal to the occipital region. These spatial profiles of alpha rhythm cannot be obtained by real-valued ICA. The phase shift phenomenon is observed because alpha rhythms smoothes through volume conductivity. The relationship between the frontal and occipital site corresponds to the direction of wave propagation. IC2 and IC3 (travelling wave [20]) have a gradient phase shift. Phase of frontal region has delay phase from the occipital region. This phenomenon indicts that source of these two alpha rhythms generated at the occipital, and direction of the wave is from occipital to frontal. IC4 (standing wave [20]) has a sudden phase shit between front and occipital. In the power aspect, alpha activity of IC4 in the central region is weak and powerful in both frontal and occipital regions. It maybe indicts that in the condition of IC4, there two coupled sources generate the oscillations with the same frequency and travel in opposite directions. A source in the deep brain region could be a node of these two oscillations (frontal and occipital cortex).

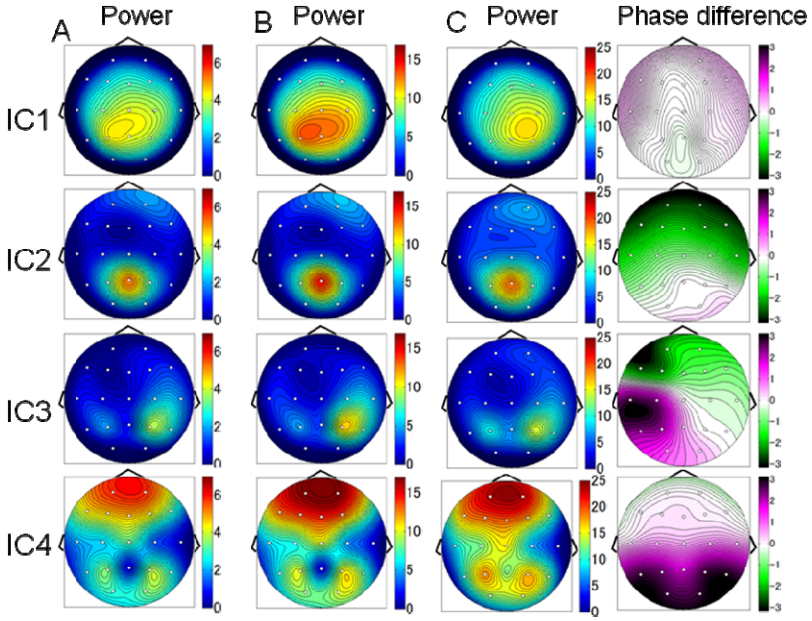

Figure 4.12 Comparison of scalp maps of decomposed alpha sources obtained by three different methods of Subject 1. (A) band-pass filter + real-valued ICA. (B) real-valued wavelet analysis + real-valued ICA. (C) complex-valued wavelet analysis + complex-valued ICA.

The comparisons between real-valued and complex-valued ICs of other subjects were shown in Figure 4.13~4.15. Because of the incomplete rejection, artifacts of neck muscle activities remained in Subject 2 (Figure 4.12 ICs 4 and 5). Except the remained artifacts, estimation of number of ICs is 3~4 according to different subjects. In the subjects selected in this paper, instantaneous mixture exist in Subject 1 (Figure 4.11, IC3) and Subject 2 (Figure 4.12, IC6), and phase lag mixture exist in all of the subjects.

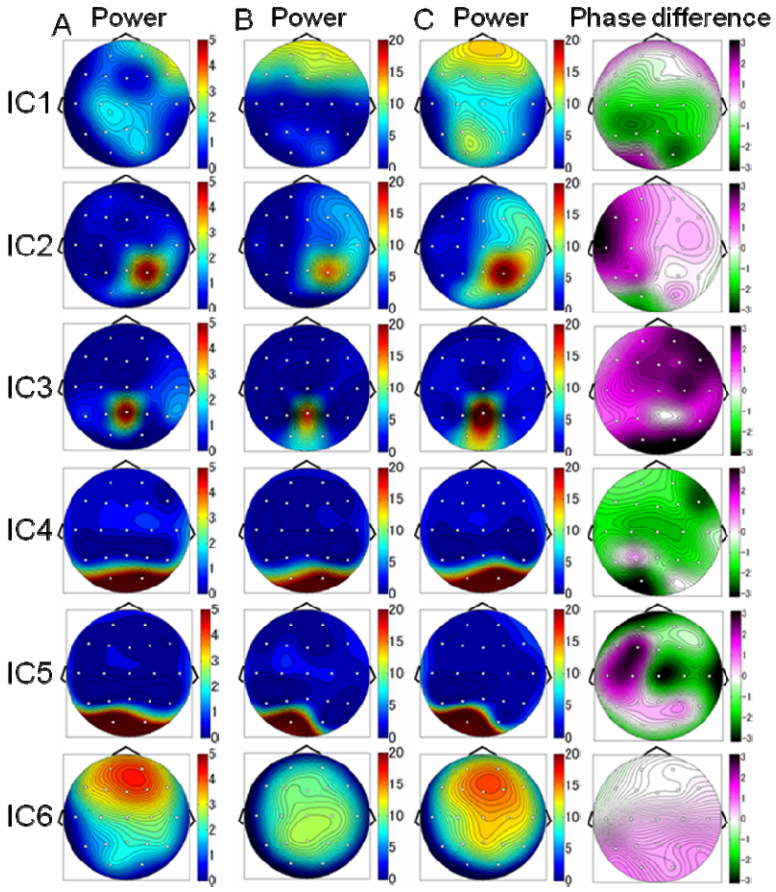

Figure 4.13 Comparison of scalp maps of decomposed alpha sources obtained by three different methods in Subject 2. (A) band-pass filter + real-valued ICA. (B) real-valued wavelet analysis + real-valued ICA. (C) complex-valued wavelet analysis + complex-valued ICA.

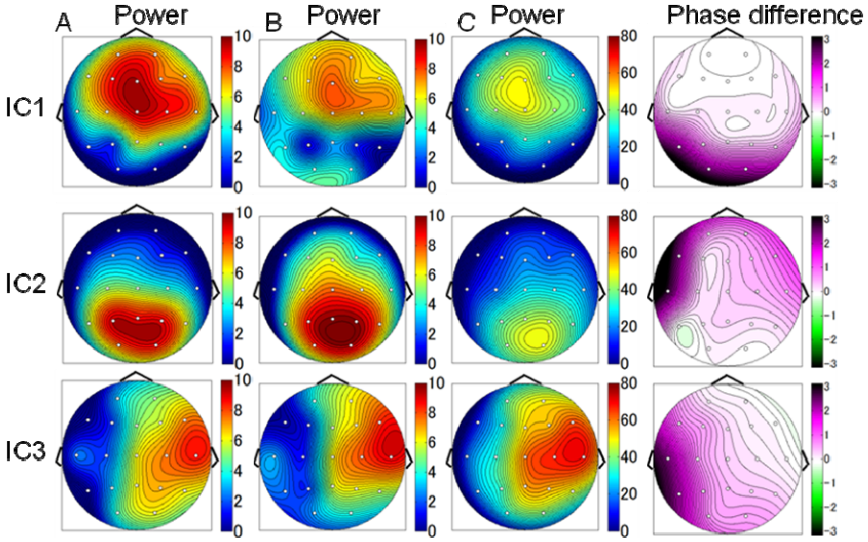

Figure 4.14 Comparison of scalp maps of decomposed alpha sources obtained by three different methods of Subject 5. (A) band-pass filter + real-valued ICA. (B) real-valued wavelet analysis + real-valued ICA. (C) complex-valued wavelet analysis + complex-valued ICA.

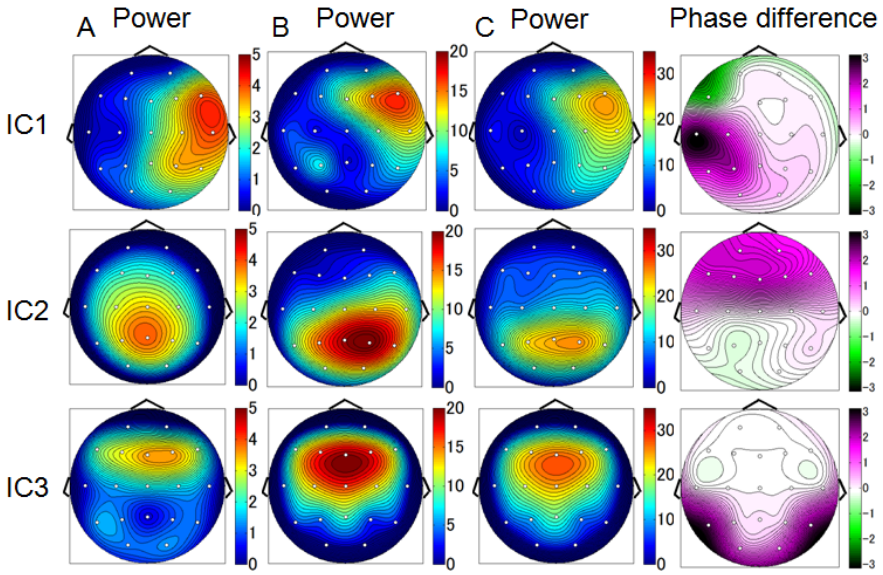

Figure 4.15 Comparison of scalp maps of decomposed alpha sources obtained by three different methods of Subject 6. (A) band-pass filter + real-valued ICA. (B) real-valued wavelet analysis + real-valued ICA. (C) complex-valued wavelet analysis + complex-valued ICA.

To compare the performance of real-valued and complex-valued ICA, we assessed the degree of separation of each algorithm by fourth order cross-cumulant described in Section 3.4.6. Figure 4.16 shows the results of cross-cumulant of 5 subjects [38]. In Subject 1 and 2, estimations of ICs number of are 4 and 6, respectively. At these estimations, the performance of complex-valued ICA are better than real-valued ICA (A and B). In Subject 5, 6 and 9, complex-valued ICA was always lower (better) than real-valued ICA (C, D and E).

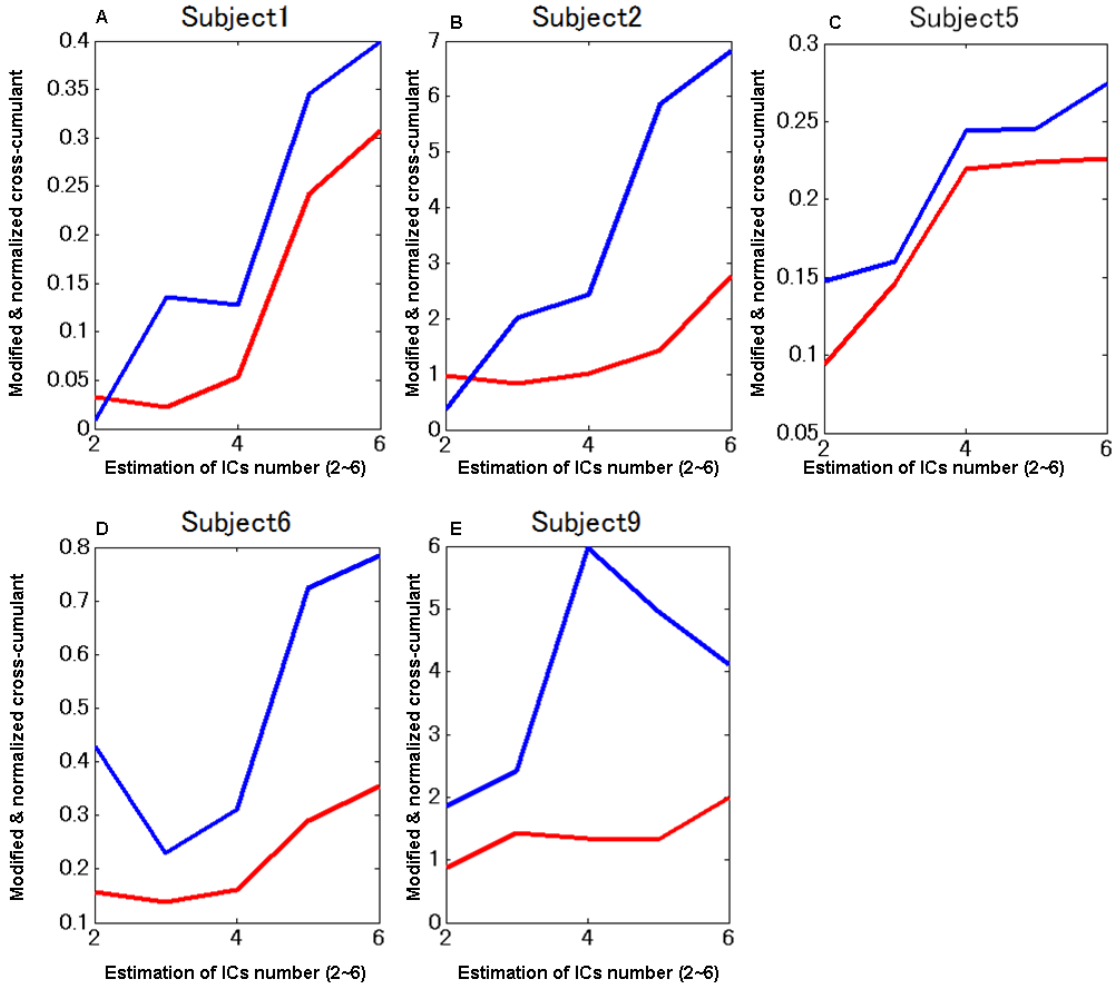

Figure 4.16 Modified and normalized cross-cumulant of five subjects (Subject 1, 2, 5, 6 and 9, blue: cross-cumulant of real-valued ICA, red: cross-cumulant of complex-valued ICA).

Method combined by wavelet analysis and complex-valued ICA presents not only power but also phase of alpha rhythm of scalp maps. Phase maps would be useful for investigation of the mechanism of cortical alpha rhythms, especially in checking the spread model of alpha rhythm on the scalp. According to the phase difference map, both instantaneous and phase-lag mixture exist between sources and electrodes in these subjects. Thus the assumption of real-valued ICA is not satisfied in these subjects. On the other hand, the degree of separation achieved by real-valued and complex-valued ICA also indicts the better performance of complex-valued ICA. On the basis of above two results, we adopted complex-valued wavelet analysis + complex-valued ICA to investigate the relationship between alpha rhythms and sleepiness.

4.4 Sleepiness and alpha rhythms

Relationship between the alpha sources (ICs obtained by complex-valued ICA) and the sleepiness of the subject were investigated. Figure 4.17 shows the time course of ICs, facial expression, driving performance and reaction time. As shown in the figure, the sleepiness scored based on the facial expression increased first, and then the driving performance got worse (i.e. absolute value of difference between the cursor and the center of road and reaction time to flush stimulation). Interestingly, the power of ICs significantly increased when the facial expression score exceed level 3 (800-1700-sec and >2300-sec).

As described in Chapter 3, we considered the wheel stopping event as the onset of sleepiness. There are 14 wheel stopping event occurred in this subject. After the calculation of event-trigger average before and after the onset of the event, we got the average waveform of ICs. We estimated the threshold by power distribution of ICs at normal wakeful time period. The threshold was set to the power of cumulative distribution got 99.9% (Figure 4.18C). We considered the ICs which power before the onset of sleepiness larger than the threshold could predict sleepiness. As shown in Figure 4.18B, only ICs 1 and 3 had the time point that power larger than threshold. The time point of IC3 larger than threshold was earlier than IC1. Thus in Subject 1, the alpha rhythm observed at right-parietal of scalp has the possibility to predict the onset of sleepiness.

We also analyzed the prediction capability of the alpha rhythms (Subject 1) separated by real-valued ICA (Figure 4.19A) and complex-valued PCA (Figure 4.20 A). In this condition, the most of powerful IC decreases (IC4), the other ICs power increase (IC2) or even generate a new IC (IC4). And the sleepiness prediction capability of IC2 also increased. According to the phase maps, assumption of real-valued ICA is not satisfied in the propagation of alpha rhythm. Thus the results separated by complex-valued analysis would be more accurate. According to the Event-triggered average of PCA (Figure 4.20), the sources separated by PCA also have the capability of predicting the sleepiness (PC2, PC3 and PC4). However, comparing with the power topographic maps of ICA, source power of PCA spread larger area. Thus it is difficult to distinguish the exact location of alpha source by PCA.

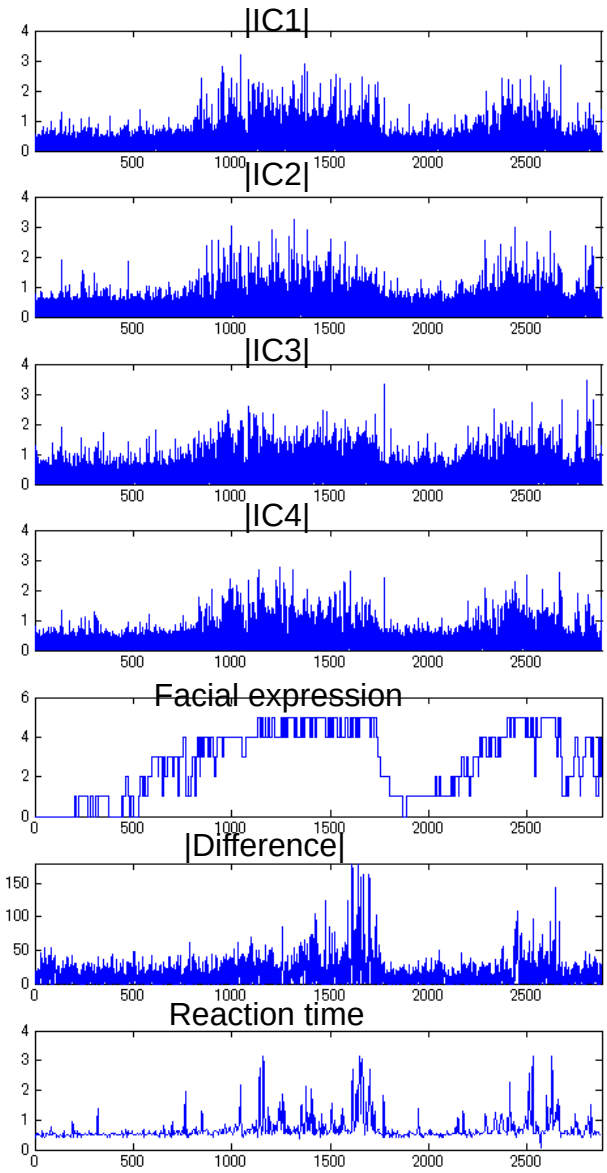

Figure 4.17 An example of a time course of the power of alpha ICs obtained by complex- valued ICA of Subject 1, facial expression score, driving performance and reaction time during the driving simulation task.

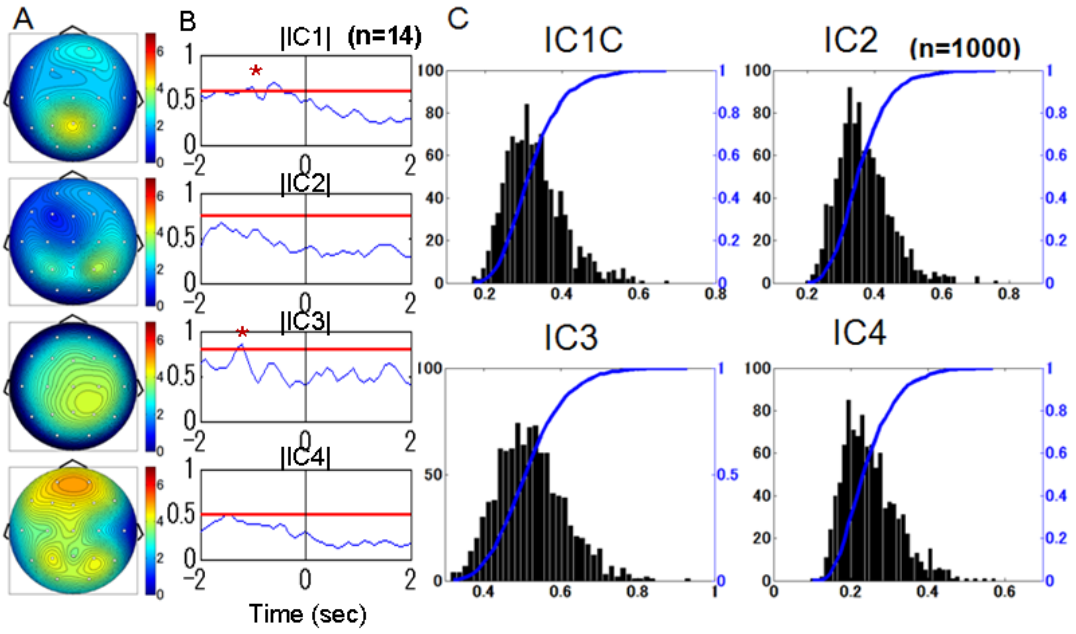

Figure 4.18 Relationship between sleepiness and alpha rhythm of Subject 1. A: topographic map of 4 ICs indicating distribution of alpha rhythm. B: event-trigger average before and after onset of no movement at wheel. (Red line: threshold) C: histogram of power distribution for each IC in wakeful time. (Blue line: cumulative distribution) each histogram based on 1000 samples estimates. Threshold is the power when cumulative distribution gets 99.9% for wakeful time.

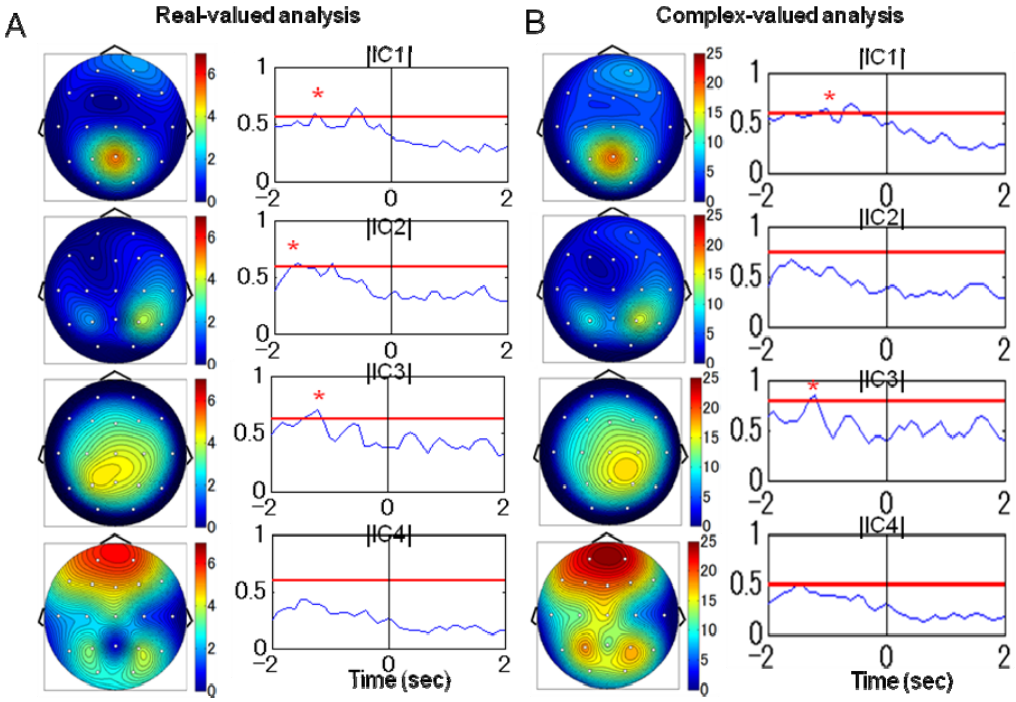

Figure 4.19 The prediction capability of alpha rhythms separated by real-valued ICA (A) and complex-valued ICA (B).

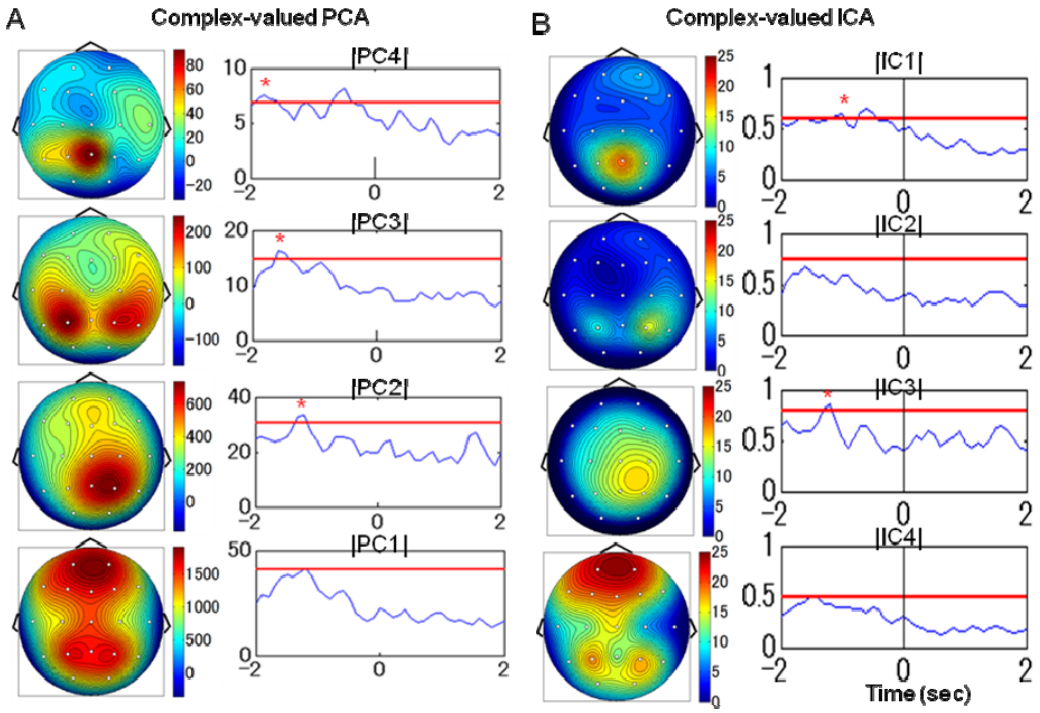

Figure 4.20. Comparison of the sleepiness prediction of alpha rhythms separated by complex-valued PCA (A) and ICA (B).

The same analysis was conducted on the data of other subjects (Figure 4.21~4.24). Except artifacts remained in Subject 2, four kinds of alpha rhythms were separated (frontal, right parietal, central-parietal and frontal-central alpha rhythms). Only the alpha rhythm whose source is right parietal could predict the onset of sleepiness. In the subjects 5 and 6, there were three kinds of alpha rhythm separated (frontal, parietal-occipital and right temporal alpha rhythms). The power of right temporal alpha rhythm exceeded the threshold earlier than other alpha rhythms. Four kinds of alpha rhythms were separated in Subject 9, including left temporal, frontal-central and two different right parietal alpha rhythms. In this subject, both of the right parietal alpha rhythms could anticipate the onset of wheel stopping.

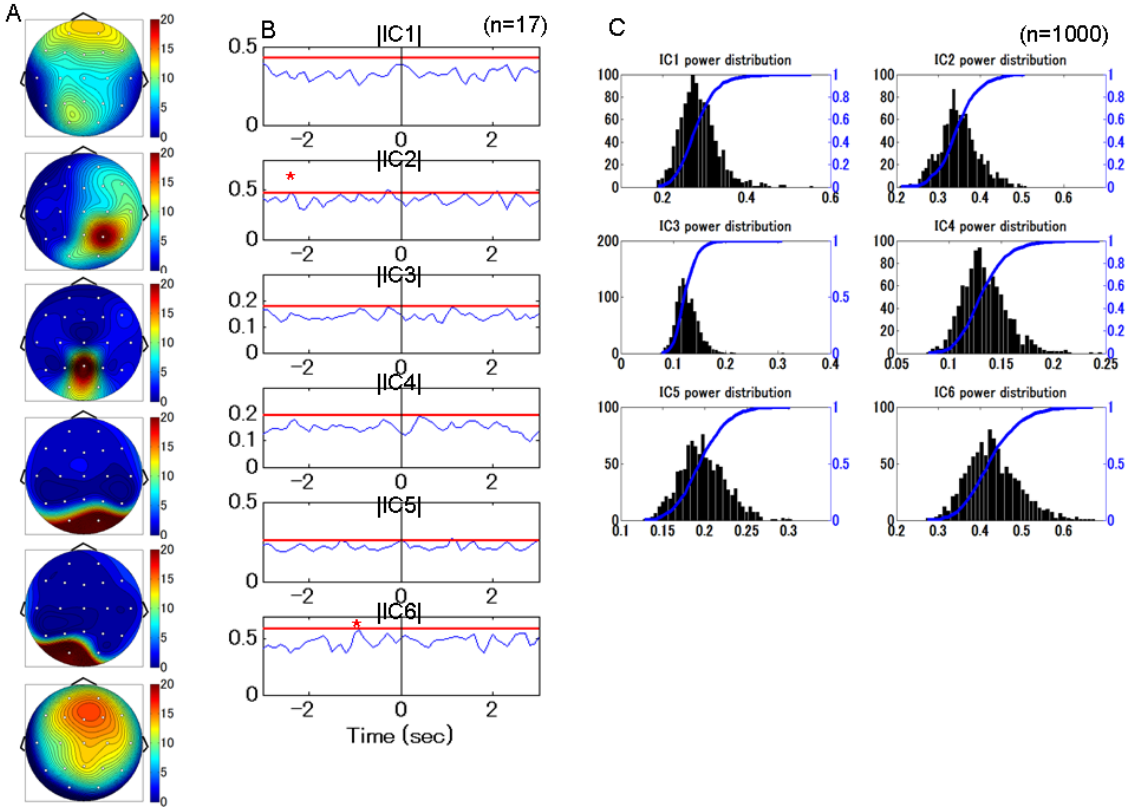

Figure 4.21 Relationship between sleepiness and alpha rhythm of Subject 2.

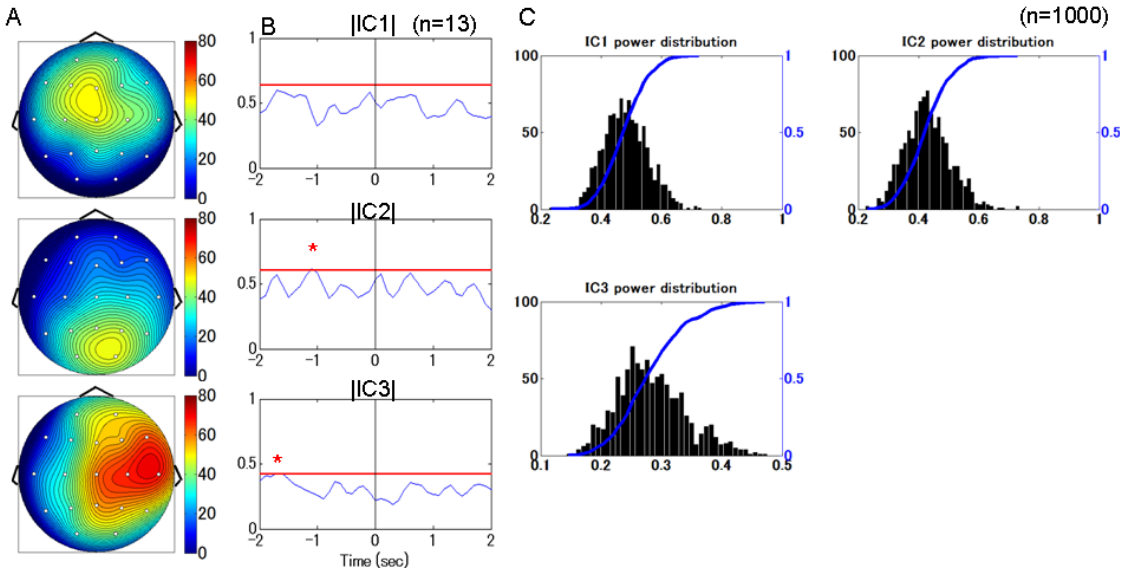

Figure 4.22 Relationship between sleepiness and alpha rhythm of Subject 5.

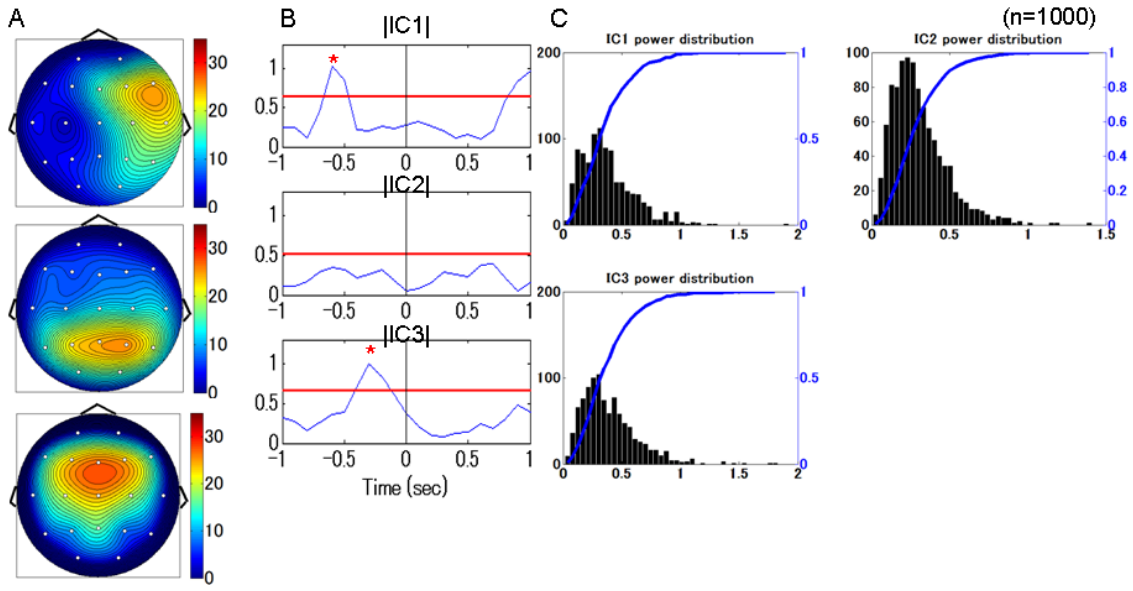

Figure 4.23 Relationship between sleepiness and alpha rhythm of Subject 6.

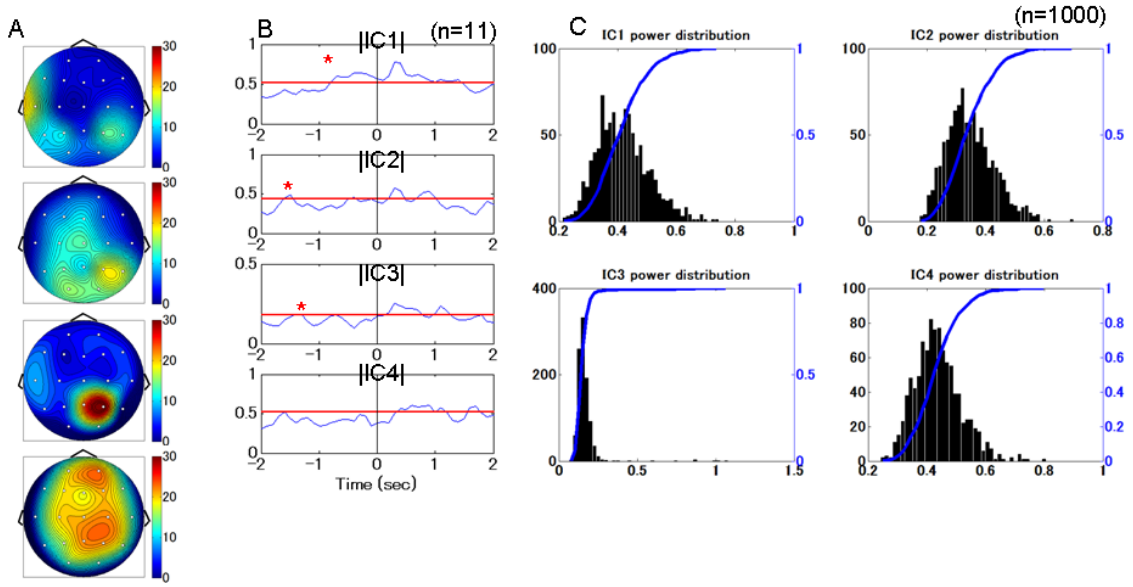

Figure 4.24 Relationship between sleepiness and alpha rhythm of Subject 9.

4.5 Summary and discussion

In the Section 4.1, the task performance was investigated. The event of wheel stopping was considered as the onset of the sleepiness. Because of the contamination of eye movement and muscle activities during the recording, we used Informax FastICA to remove noise from EEG signals. We got the corrected EEG signals by projecting the ICs

onto scalp after rejecting the artifacts. The corrected EEG signals were almost free of the artifacts. The alpha-band sources were decomposed by real-valued ICA and complex-valued ICA in Section 4.3. In addition, phase maps can be obtained by complex-valued ICA is suggested to provide useful information about the generation mechanism of alpha EEG. Cross-cumulant analysis between decomposed sources suggested degree of separation indicated the better performance of complex-valued wavelet analysis + complex-valued ICA to separate the alpha rhythms of human.

Section 4.3 demonstrated the possibility of prediction of the onset of sleep by the alpha EEG signals. According to results of the 5 of 13 subjects, we divided the subjects into two groups as Figure 4.25 Separated alpha rhythms whose sources are at right parietal of the scalp in Group 1 (Subject 1, 2 and 9) can predict onset of sleepiness earlier than others. The right temporal alpha rhythm separated in Group 2 (Subject 5 and 6) is useful for prediction of onset of sleepiness. The analyzed data length of each subject is: 193.7-sec (Subject 1), 28.7-sec (Subject 2), 13.7-sec (Subject 5), 25.8-sec (Subject 6) and 107.5-sec (Subject 9). The shorter sample length of Group 2 has the possibility that could not represent the EEG activity during 2880-sec driving simulation. Thus the result of sleepiness prediction capability of alpha rhythms in Group 1 is more credible, which means the alpha rhythm at right parietal of scalp can predict the onset of sleepiness.

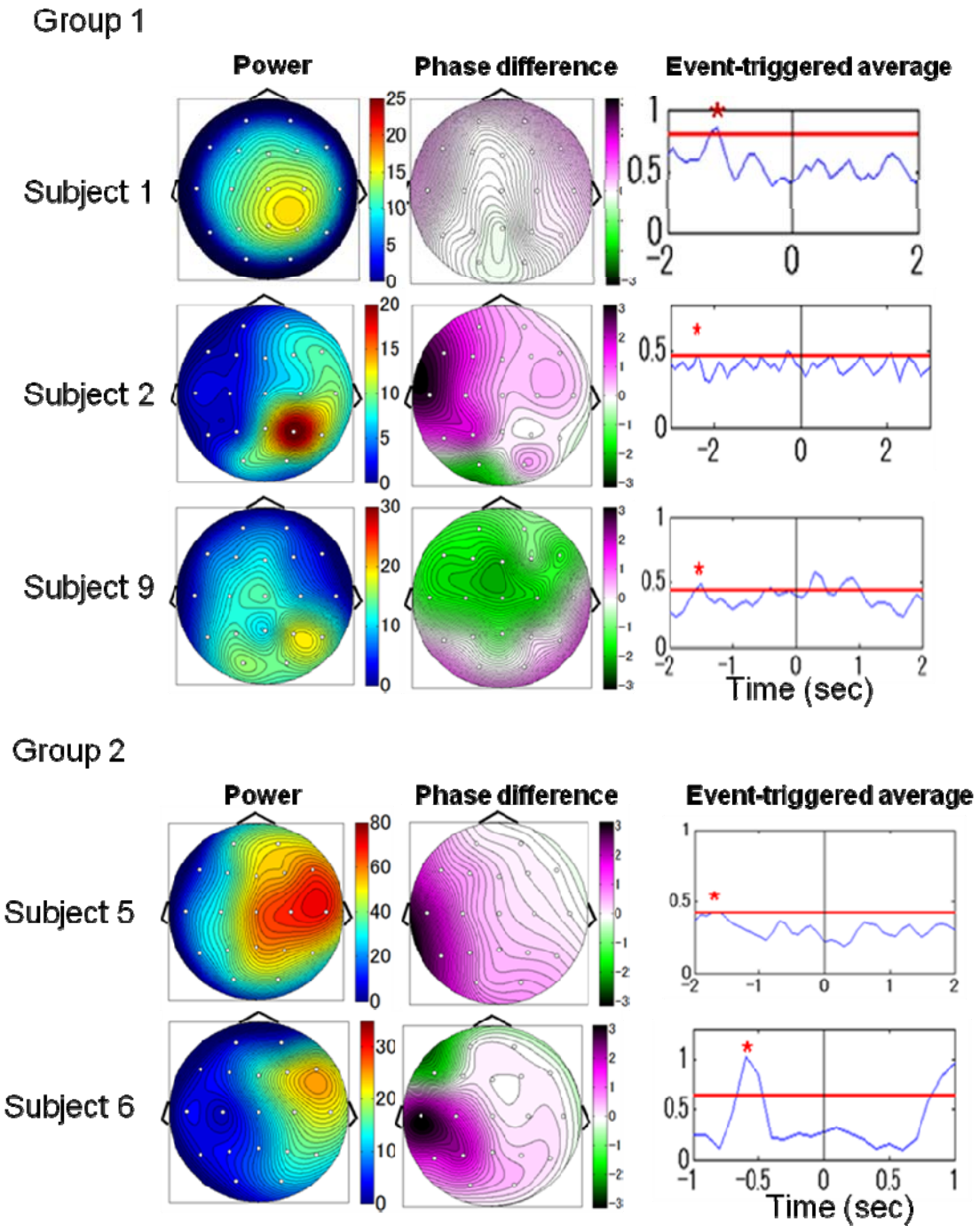

Figure 4.25 Groups divided according the relationship between alpha rhythm and sleepiness.

Chapter 5 Conclusion

In this study, we proposed a method to decompose the source of EEG alpha rhythms by the combination of continuous wavelet analysis and complex-valued ICA. We investigated the relationship between the separated ICs, which were considered alpha rhythm sources, and sleepiness.

Our method proved not only the power but also the phase of alpha rhythms of scalp map of alpha sources. Therefore, the phase difference between the recording sites can be naturally represented as the scalp maps. The phase map would be useful for the investigation of the mechanism of cortical alpha rhythms, in particular dipole estimation of alpha sources in the brain. In the subject we analyzed, both instantaneous and phase-lag mixture exist between sources and electrodes. The assumption of instantaneous mixture is not satisfied in our research. On the other hand, the degree of separation also indicted the better performance than real-valued ICA. Thus the method combined by complex-valued wavelet analysis and complex-valued ICA is proved to be useful for separating the alpha rhythms.

At last, we investigated the relationship between sleepiness and distribution of alpha rhythm separated by complex-valued ICA. According to the previous research on the scalp map of alpha rhythms, it is suggested that an increase in the alpha power in the central area leads increase in the subjective sleepiness [26]. In our study, we selected 5 subjects to analyze the prediction of alpha rhythms for sleepiness. According to different subjects, results were divided into 2 groups. Because of the larger contribution of alpha rhythms in Group 1, the right parietal alpha rhythm in Group 1 has the possibility to predict the onset of sleepiness.

In this study, in order to prevent the driving sleepiness, we analyzed the relationship between the alpha rhythms separated by complex-valued method and sleepiness. As the result, it is indicted that right parietal alpha rhythm has the prediction capability for sleepiness.

The research about alerting the sleepiness of driver is very meaningful for reducing the fatal accidents and saving lives. Although the result of my study indicts the usefulness for predicting the sleepiness, further studies will be required to automatically determine the number of ICs. And study of judging the exact timing of sleepiness onset is also required.

Acknowledgment

This work is done during my studying at laboratory of biomodeling, Graduate Schllo of Information Science (GSIS), Tohoku University, from April, 2008 to March, 2010.

I am deeply indebted to Professor of Biomodeling Laboratory, Prpfessor Dr. M. Nakao for giving me the permission to study in Japan and in this laboratory. And I deeply appreciate his recommendation for me to get the scholarship of ASIST, which helped me to focus on studying Japanese and doing the research.

I would like to thank Professor Dr. Y. Suzuki and from Research Institute of Electrical Communication and Professor Dr. T. Yoshinobu from Graduate School of Engineering. Their extensive advices around my work have been very helpful.

I owe my most sincere gratitude to my supervisor, Associate Professor Dr. N. Katayam, for his generous support either in research or in daily life. Without his help, I could not finish my master studying in Japan. He provided me encouragement and support in various ways. I would never forget he checked my paper the whole night before the submission of MBE conference and the practices for my presentation every time until after midnight. Besides the studying, he also helped me to check the entry sheet for my job hunting and I finally received the offer from a Japanese company. In an addition, he helped me to improve my Japanese on E-mail verbiage and honorific expression which will be helpful for my future life as an employee. I would never forget the Japanese company culture he taught me such as “報、連、相”. His truly scientist intuition, passion of research and dignified personality inspires and enrich my growth a student and a human being. I respect him from my heart.

I really appreciate the help from Assistant Professor Dr. A. Karashima in my laboratory. He always helped me when I had problems with the results of his student and contact with DENSO Corporation Research Laboratory to get the information of system.

Thanks for the DENSO Corporation Research Laboratory for supplying the experiment and data.

I also want to express my gratitude for the helps from the other members in my laboratory. All their kindness makes my study life in Japan a beautiful memory. Many thanks go in particular to Mr. Shiraishi and the other M2s for helping me a lot.

Lastly, I would like to thank my parents for their support.

References

[1] Royal Society for Prevention of Accidents, “Driver fatigue and road accidents: a literature review and position paper”, The Royal Society for the Prevention of Accidents, 2001.

[2] Y. Tojima, T. Sakura, “Investigation concerning the relation between sleepiness and traffic accident in taxi drivers”, *Japanese society of occupational medicine and traumatology*, vol. 54, pp.43-47, 2006.

[3] L. Torsvall, T. Akerstedt, “Sleepiness on the job: continuously measured EEG changes in train drivers”, *Electroenceph. Clin. Neurophysiol*, vol. **66**, pp.502-511, 1987.

[4] C. Papadelis, Z.Chen, C. K. Papadelis, P. Bamidis, I, Chouvards, E. Bekiaris, N, Maglaveras, “Monitoring sleepiness with on-board electrophysiological recordings for preventing sleep-deprived traffic accede- nts”, *Clin. Neurophysiol*, vol. **118**, pp.1906-1922, 2007.

[5] H. Berger, “Ueber das Elektroenkephalogramm des Menschen”, *Nervenkrankheiten*, vol. **87**, pp.527- 570, 1929.

[6] H. Jasper, H. Andrews, “Normal differentiation of occipital and precentral regions in man”, *Arch Neurol Psychiatry*, vol. **39**, pp.96-115, 1938.

[7] E. Niedermeyer, “Alpha-like rhythmical activity of the temporal lobe”, *Clin Electroencephalogr*, vol. **21**, pp.210-224, 1990.

[8] T. Nilsson, T. M. Nelson, D. Carlson,”Development of fatigue symptoms during simulated driving”, *Accid. Anal.* Prev. 29 (4), 479-488, 1997.

[9] J. C. Miller, R. R. Mackie, “Effects of irregular schedules and physical work on commercial driver fatigue and performance”, *Human Factors in Transport Research. Academic Press*, pp.127-133, New York, 1980.

[10] Z. Zhang, N. Katayama, K. Watanabe, H. Nakatani, A. Karashima, M. Nakao, “A Topographic Analysis of Human Scalp Alpha EEG by the Complex-valued ICA”, *IEICE Tech. Rep*., *MBE2009-69*, vol. **109**, no. 279, pp.41-46, Nov. 2009.

[11] C. J. Reissman, “The alert driver: a trucker’s guide to sleep, fatigue, and rest in our 24-hour society”, American Trucking Associations, USA, 1996.

[12] Safety Study, “Factors that affect fatigue in heavy truck accidents”, National Transportation Safety Board, Washington, USA.

[13] A. M. Ivanitsky, A. R. Nikolaev and G. A. Ivanitsy, “Electroencephalography”, *Modern Techniques in Neuroscience Research*, pp.971-991, 1999.

[14] S. W. Hughes and V. Crunelli, “Thalamic mechanisms of EEG alpha rhythm and their pathological implications”, *Neuroscientist*, 2005.

[15] L. Torsvall, Y. Akerstedt, “Sleepiness on the job: continuously measured EEG changes in train drivers”, *Electroencephalogr Clin. Neurophysiol*, vol. **66**, pp.502 -511 ,1987.

[16] J. Santamaria, K. H. Chiappa, “The EEG of drowsiness in normal subjects”, *J. Clin. Neurophysiol*, vol.**4**, pp. 327-382, 1987.

[17] S. K. L. Lal, A. Craig, “Psychophysiological effects associated with drowsiness: driver fatigue and electroencephalography”, *Int. J. Psychophysiol*, 2000(abstract).

[18] O. N. Markand, “Alpha rhythm”, *J. Clin. Psychophysiol*, vol. **7**(2), 163-189, 1990.

[19] A. Hyvärinen, J. Karhunen, and E. Oja, Independent Component Analysis, S. Haykin, ed., Wiley- Interscience Publication, USA, 2001.

[20] J. Ito, A. R. Nikolev, C. Leeuwen, “Spatial and temporal structure of phase synchronizationof spontaneous alpha EEG activity”, *Biol. Cybern*. vol. **92**, pp.54-60, 2005.

[21] S. D. Baulk, L. A. Reyner, J. A. Horne, “Driver sleepiness-evaluation of reaction time measurement as a secondary task”, *Sleep*, vol. **24**, pp.695-698, 2001.

[22] H. Kitajima, N. Numata, K. Yamamoto, Y. Goi, Prediction of Automobile Driver Sleepiness: 1st Report, Rating of Sleepiness Based on Facial Expression and Examination of Effective Predictor Indexes of Sleepiness [in Japanese], *Trans Japan Soc Mech Eng*. (Book C), vol. **63**, pp.3059-3066, 1997.

[23] T. Kimura, K. Ishida, N. Ozaki, “Feasibility Study of Sleepiness Detection Using Expression Features”, *Rev Automotive Eng*. vol. **29**, pp.567-574, 2008.

[24] H. H. Jasper. “The ten-twenty electrode system of the international federation”, *Electroen-cephalography and Clinical Neurophysiology*, vol. **10**, pp.371-373, 1958.

[25] M. Brown, M. Marmor and Vaegan, “Stadnard for clinical electro-oculography”, *Documenta Ophthalmologica*, vol. **113**, pp.205-212, 2006.

[26] K. Watanabe, H. Nakatani, A. Karashima, N. Katayama, M. Nakao, “Instantaneous theta and alpha rhythm of EEG is related to impairment of drive performance in humans”, *Annual Meeting of Society for Neuroscience*, Nov.2008.

[27] J. N. Knight, Signal fraction analysis and artifact removal in EEG, Colorado State University, 2003.

[28] P. Anderer, S. Roberts, A. Schlogl, G. Gruber, G. Klosch, W. Herrmann, P. Rappelsberger, O. Filz, M. J. Barbanoj, G. Dorffner and B. Saletu, “Artifact Processing in Computerized Analysis of Sleep EEG - A Review”, *Neuropsychobiology*, 1999.

[29] P. Anderer, H. V. Semlitsch, B. Saletu, M. J. Barbanoj, “Artifact processing in topographic mapping of electroencephalographic activity in neuropsychopharmacology” *Psychiatry Res*, vol. **45**, pp.79–93, 1992.

[30] H. Eskola, “Utilization of MRI Information in EEG Studies”, *IJBEM*, vol.**1,** pp.54-61, 1999.

[31] D.P. Brunner, R. C. Vasko, C. S. Detka, J. P. Monahan, Reynolds CF, D. J. Kupfer, “Muscle artifacts in the sleep EEG: Automated detection and effect on all-night EEG power spectra”, *J. Sleep Res*, vol.**5**, pp.155-164, 1996.

[32] J. Hasan, “Automatic analysis of sleep recordings: A critical review”, *Ann Clin Res*, vol. **17**, pp.280-287, 1985.

[33] W. T. Blume, M. Kaibara, G. B. Young, “Atlas of Adult Electroencephalography”, Lippincott Williams and Wilkins, Philadelphia, 2002.

[34] T. Jung, C. Humphries, T. Lee, S. Makeig, M. J. McKeown, V. Iragui, T. J. Sejnowski, “Extended ICA removes artifacts from electroencephalographic recordings”, *Advances in neural information processing systems*. vol. **10**, pp.894-900, Denver, USA, 1998.

[35] H. Sawada, R. Mukai, S. Araki, and S. Makino, “Polar coordinate based nonlinear function for frequency-domain blind source separation”, Proc. ICASSP 2002, pp.1001-1004, 2002.

[36] H. Li and T. Adali, “Complex-valued adaptive signal processing using nonlinear functions”, *Transactions on Signal Processing*, vol. **51**, pp. 2540-2549, 2003.

[37] T. D. Sandwell, “Biharmonic spline interpolation of geo-3 and seasat altimeter data”, *Geophysical Research Letters*, vol. **14**, pp. 139-142, 1987.

[38] J. Anemuller, T. J. Sejnowski, S. Makeig, “Complex independent component analysis of frequency-domain electroencephalographic data”, *Neural Networks*, vol. **16**, pp. 1311-1323, 2003.

[39] P. D. Welch, "The use of fast fourier transform for the estimation of power spectra: a method based on time averaging over short, modified periodograms", *IEEE Trans. Audio Electroacoustics,* vol. 15, pp.70-73, 1967.

Publication

Z. Zhang, N. Katayama, K. Watanabe, H. Nakatani, A. Karashima, M. Nakao, “A Topographic Analysis of Human Scalp Alpha EEG by the Complex-valued ICA”, *IEICE Tech. Rep.*, *MBE2009-69*, vol. **109**, no. 279, pp.41-46, Nov. 2009.